Mon. Not. R. Astron. Soc. **000**, 1–19 (2011) Printed 28 January 2013 (MN LaTeX style file v2.2)

arXiv:1106.1630v1 [astro-ph.HE] 8 Jun 2011

Faraday Conversion And Rotation In Uniformly Magnetized Relativistic Plasmas

Lei Huang[1,2]* and Roman V. Shcherbakov[3]

[1] *Key Laboratory for Research in Galaxies and Cosmology, Shanghai Astronomical Observatory, Chinese Academy of Sciences, Shanghai 200030, China*

[2] *Key Laboratory of Radio Astronomy, Chinese Academy of Sciences*

[3] *Harvard-Smithsonian Center for Astrophysics, 60 Garden Street, Cambridge, MA 02138, USA*

28 January 2013

ABSTRACT

We provide precise fitting formulae for Faraday conversion and rotation coefficients in uniformly magnetized relativistic plasma. The formulae are immediately applicable to Rotation Measure and Circular Polarization (CP) production in jets and hot accretion flows. We show the recipe and results for arbitrary isotropic particle distributions, in particular thermal and power-law. The exact Faraday conversion coefficient is found to approach zero with the increasing particle energy. The non-linear corrections of Faraday conversion and rotation coefficients are found essential for reliable CP interpretation of Sgr A*.

Key words: plasmas – polarization – radiation mechanisms: general – radiative transfer – Galaxy: centre

1 INTRODUCTION

The cyclo-synchrotron emission, also called magneto-bremsstrahlung emission, is one of the most important radiative mechanism in astrophysics. It is believed to produce radio emission in the centers of AGNs and LLAGNs (low luminosity AGNs, such as the Galactic Center). A polarized nature of cyclo-synchrotron emission is of increasing interest for radio observers. With the help of polarization one can understand the magnetic field structure in radio sources. Basic theory of emission and propagation of polarized light has been established (e.g., Legg & Westfold 1968; Pacholczyk 1970; Jones & O'Dell 1977). Particles in cold plasma emit cyclotron radiation, which is circularly polarized (CP). When linearly polarized (LP) light propagates through cold magnetized plasma, it undergoes Faraday rotation. In turn, relativistic plasma emits synchrotron radiation, which is linearly polarized. Light traversing relativistic plasma undergoes both Faraday conversion and Faraday rotation.

In simple theory the strength of Faraday rotation effect is proportional to $\lambda^2 n_e \boldsymbol{B}\cdot\delta\boldsymbol{l}$, where λ is the photon wavelength, n_e is electron density, $\boldsymbol{B}$ is magnetic field vector, and $\boldsymbol{l}$ is the displacement along the line of sight. However, Trubnikov (1958) and Melrose (1997a) have shown that in a general case Faraday rotation of plasma depends also on the Lorentz factor of electrons γ. Faraday rotation weakens with the increase of γ as $\ln\gamma/\gamma^2$. The electric vector position angle (EVPA) of LP light will be preserved better, if the electrons are relativistic. Thus we can infer the intrinsic EVPA of a synchrotron-emitting source. The electrons in the vicinity of a black hole Sagittarius A* (Sgr A*) in Galactic Center are often modeled by a relativistic Maxwellian (thermal) distribution with temperature $> 10^{10}$K (e.g. Yuan, Quataert & Narayan 2003). When Faraday rotation is strong and non-uniform across the beam, then beam depolarization can diminish the resultant LP fraction (Bower et al. 2005). The effect of large Lorentz factors on Faraday rotation measure near Sgr A* must be considered to explain the detected LP fluxes in sub-millimeter to near-infrared bands (Quataert & Gruzinov 2010). Previous work (e.g. Ginzburg 1964; Sazonov 1969; Melrose 1997b) also highlighted Faraday conversion, or generalized Faraday rotation. This quantity describes the interconversion of linearly and circularly polarized light. It is normally expected (Homan et al. 2009) to convert emitted LP light into CP light during propagation in magnetized medium. This is the likely cause of observed high CP fraction of Sgr A* spectrum in radio band (Bower et al. 2002) and sub-millimeter band (Munoz et al. 2011).

---

* E-mail: muduri@shao.ac.cn

The strength of Faraday conversion was found proportional to $\lambda^3 n_e B^2 \sin^2\theta\delta l$, where θ is the angle between $\boldsymbol{B}$ and $\delta\boldsymbol{l}$ (or $\boldsymbol{k}$, see in Figure 1). Additional suggested proportionality to electron temperature T_e makes Faraday conversion reach very large values in relativistic plasmas. However, this proportionality ceases at very high T_e and Faraday conversion measure approaches zero (Shcherbakov 2008). A detectable CP fraction can be generated near Sgr A* in sub-millimeter band (e.g. Ballantyne, Ozel & Psaltis 2007), but precise treatment of Faraday rotation and conversion is essential (Shcherbakov et al. 2010). A non-zero CP fraction is already detected with SMA (Munoz et al., 2011, ApJ, submitted) at 230 GHz and 345 GHz. This by itself points in the direction of a very hot radiatively inefficient accretion flow (RIAF). The origin of CP near Sgr A* and jets was quantified by Beckert (2003); Shcherbakov et al. (2010). Yet more detailed and accurate calculations are needed to quantify the circular polarizations for the Galactic Center (GC) supermassive black hole and other radio source.

Huang et al. (2009) was the first to incorporate Faraday rotation and conversion within general relativistic (GR) polarized radiative transfer framework, though with some approximations. Shcherbakov & Huang (2011, hereafter Paper I) provided a method to accurately calculate cyclo-synchrotron absorption and Faraday conversion/rotation for electrons in isotropic thermal distribution and outlined the exact procedure for polarized radiative transfer in GR. Precise Faraday rotation and conversion coefficients were computed earlier for thermal plasmas in Shcherbakov (2008). An important cornerstone in computing propagation effects is linear approximation, in which only the first non-zero terms in series expansion in Ω_0/ω ratio are taken for correspondent quantities (e.g. formula 47). It was also derived therein and found consistent with result provided by Melrose (1997b). The precise values of Faraday conversion coefficient in Shcherbakov (2008) and Paper I match the linear approximation from cold to weakly-relativistic regimes of thermal plasma. In relativistic regime Faraday conversion largely deviated from the linear approximation, because it breaks at finite ratio of Ω_0/ω. Here $\Omega_0 = eB/(m_e c)$ is the cyclotron frequency and ω is the radiation frequency. Due to the lack of full investigation of various electron distributions, the important question was left unanswered: is thermal distribution special or such behavior of Faraday conversion is generic?

In present paper we expand the computations of Faraday conversion and rotation coefficients to non-thermal particle distributions. We compute the absorption coefficients as well with the same unique method. We find solutions of the wave equation and natural modes from cold limit to ultra-relativistic limit. Our formulae are precise at all reasonable particle γ's. We find a large discrepancy, if the linear approximations to Faraday conversion and rotation are used, thus justifying the need for precise computations. To be practical we adopt δ-function energy distribution of electrons and provide the fitting formulae, which can then be integrated over any isotropic distribution of particles. We also provide public code in Mathematica 8 to numerically compute the integrals. The paper is organized as follows. We derive dielectric tensor and dispersion relations for uniformly magnetized relativistic plasma with isotropic monoenergetic particle distribution in §2. The properties of natural modes are investigated in §3. In §4 we provide simplified formulae and generalize to arbitrary electron energy distributions. on its polarization prediction is described In §5 we show that the polarized spectrum changes a lot, when linear approximations are used for Sgr A* modeling.

2 RESPONSE TENSOR AND EIGENMODES OF UNIFORMLY MAGNETIZED RELATIVISTIC PLASMAS WITH δ-FUNCTION ENERGY DISTRIBUTION

2.1 Geometry and definitions

Let us define a coordinate system in three-dimensional flat space with $\boldsymbol{e}_1$ along the major axis of the synchrotron radiation ellipse, $\boldsymbol{e}_2$ along the minor axis, and $\boldsymbol{e}_3$ towards the observer (see Figure 1). Vector $\boldsymbol{e}_1$ is perpendicular to $\boldsymbol{B}$. This coordinate system is right-handed, i.e., the observer finds a counter-clockwise rotation from $\boldsymbol{e}_1$ to $\boldsymbol{e}_2$. We define Minkowski space-time with basis e^μ_α, so that $e^\mu_0 = (-1, 0, 0, 0)$ and $e^\mu_j = (0, \boldsymbol{e}_j), j = 1, 2, 3$. Unlike in Paper I, here we perform all derivations in spatial basis $(\boldsymbol{e}_1, \boldsymbol{e}_2, \boldsymbol{e}_3)$, instead of $(\tilde{\boldsymbol{e}}_1, \tilde{\boldsymbol{e}}_2, \tilde{\boldsymbol{e}}_3)$. In latter basis $\tilde{\boldsymbol{e}}_1 = \boldsymbol{e}_1$ and $\tilde{\boldsymbol{e}}_3 \parallel \boldsymbol{B}$. We set the speed of light to unity $c = 1$.

Normalized vectors of electric field in a transverse wave are

$$\hat{\boldsymbol{E}}_1 \;=\; \boldsymbol{e}_1 \;\; \mathrm{e}^{\imath(kX)} \quad \text{and} \quad \hat{\boldsymbol{E}}_2 \;=\; \boldsymbol{e}_2 \;\; \mathrm{e}^{\imath(kX)}, \tag{1}$$

where $k_\mu = \omega(-1, 0, 0, 1)^{\mathrm{T}}$ is the covariant photon momentum, X^μ are four-coordinates, and kX represents the inner product $kX = k_\mu X^\mu$. The projections of electric field $\boldsymbol{E}$ of an arbitrary wave along these unit vectors have complex amplitudes $\widetilde{A}^{1,2}$, or real amplitudes $A^{1,2}$ and phases $\delta^{1,2}$, so that

$$\boldsymbol{E} = \boldsymbol{E}_1 + \boldsymbol{E}_2 = \widetilde{A}^1\hat{\boldsymbol{E}}_1 + \widetilde{A}^2\hat{\boldsymbol{E}}_2 \quad = \quad A^1\mathrm{e}^{i\delta^1}\hat{\boldsymbol{E}}_1 + \quad A^2\mathrm{e}^{i\delta^2}\hat{\boldsymbol{E}}_2. \tag{2}$$

The tensor of intensity is defined as

$$\mathcal{I}_{ij} =< \boldsymbol{E}_i \cdot conj[\boldsymbol{E}_j] >, \tag{3}$$

where $conj[...]$ stands for complex conjugate and $<>$ represents the average over the wave ensemble.

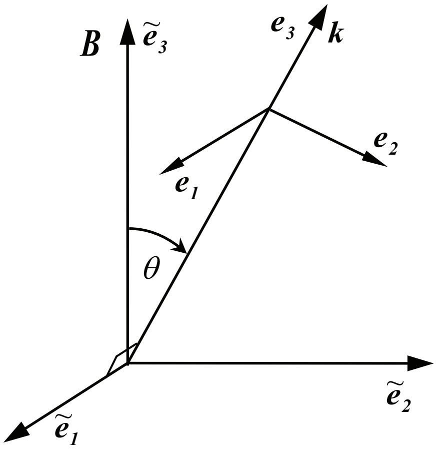

Figure 1. Geometry of the problem. Vector $\boldsymbol{B}$ represents uniform magnetic field. The transverse plane wave travels along $\boldsymbol{k}$ and has electric field $\boldsymbol{E}$ in $(\boldsymbol{e}_1, \boldsymbol{e}_2)$ plane.

Radiative transfer in uniform medium is described by the equation (Sazonov 1969)

$$\frac{\omega}{2\pi}\cdot\frac{\mathrm{d}}{\mathrm{d}s}\mathcal{I}_{ij} \quad = \quad \varepsilon_{ij} \quad + \quad i(\alpha^{im}\mathcal{I}_{mj} - \alpha^{*jn}\mathcal{I}_{in}), \tag{4}$$

where s is the distance along the ray, ε_{ij} is the tensor of spontaneous emission and α^{ij} is the tensor of wave propagation, or the response tensor. The equation (4) can be rewritten in a more familiar form (Shcherbakov & Huang 2011)

$$\frac{d\boldsymbol{S}}{ds} = \begin{pmatrix} \varepsilon_I \\ \varepsilon_Q \\ 0 \\ \varepsilon_V \end{pmatrix} - \begin{pmatrix} \eta_I & \eta_Q & 0 & \eta_V \\ \eta_Q & \eta_I & \rho_V & 0 \\ 0 & -\rho_V & \eta_I & \rho_Q \\ \eta_V & 0 & -\rho_Q & \eta_I \end{pmatrix} \boldsymbol{S} \tag{5}$$

with the polarization vector

$$\boldsymbol{S} = (I, Q, U, V)^T \tag{6}$$

being the vector of Stokes parameters. The intensities $\boldsymbol{S}$ and integrated polarized fluxes can be directly observed. Here $\varepsilon_I, \varepsilon_Q, \varepsilon_V$ are the emission coefficients,

$$\begin{aligned} \eta_I &= \mathrm{Im}(\alpha^{22} + \alpha^{11})/\nu, \\ \eta_Q &= \mathrm{Im}(\alpha^{11} - \alpha^{22})/\nu, \\ \eta_V &= 2\mathrm{Re}(\alpha^{12})/\nu, \end{aligned} \tag{7}$$

are the absorption coefficients,

$$\begin{aligned} \rho_V &= 2\mathrm{Im}(\alpha^{12})/\nu, \\ \rho_Q &= \mathrm{Re}(\alpha^{22} - \alpha^{11})/\nu, \end{aligned} \tag{8}$$

where $\nu = \omega/(2\pi)$ is the frequency. In the following we will concentrate mainly on Faraday rotation coefficient ρ_V and Faraday conversion coefficient ρ_Q, which are generally called propagation coefficients. They directly influence the observed polarized fluxes.

2.2 Response tensor and dispersion relations

We start with the formula for the response tensor for isotropic electrons

$$\alpha^{\mu\nu}(k) = -\frac{e^2}{m_e c}\int \mathrm{d}^3\mathrm{p}\frac{\mathrm{d}f(\gamma)}{\mathrm{d}\gamma}\widetilde{\mathcal{U}}^\mu\widetilde{\mathcal{U}}^\nu + \frac{\imath e^2\omega}{m_e c}\int_0^\infty \mathrm{d}\xi t^\nu_\sigma(-\xi)\left[\frac{\partial^2}{\partial\mathcal{S}_\mu\partial\mathcal{S}_\sigma}\int \mathrm{d}^3\mathrm{p}\left(-\frac{1}{\gamma}\frac{\mathrm{d}f(\gamma)}{\mathrm{d}\gamma}\mathrm{e}^{-\imath\mathcal{R}(\xi)\mathcal{U}+\mathcal{S}\mathcal{U}}\right)\right]_{\mathcal{S}_\mu=0}, \tag{9}$$

where $\widetilde{\mathcal{U}}^\mu = (1,0,0,0)$, $\mathcal{U}^\mu$ is 4-velocity of electrons in observer's Minkowskian frame, p is dimensionless 3-momentum defined as $\mathrm{p} = \sqrt{\gamma^2 - 1}$, and $f(\gamma)$ is the energy distribution function of electrons. It is normalized to the number density of electrons n_e as

$$\int f(\gamma)\mathrm{d}^3\mathrm{p} = n_e. \tag{10}$$

Tensor $\dot{t}^{\mu\nu}(\xi)$ describes how the velocity of electrons changes with proper time ξ, $\mathcal{R}(\xi)\mathcal{U}$ represents the difference of the phase (kX) of the electron, and $\mathcal{S}_\mu$ is an auxiliary variable. The formula (9) coincides with Eq. (2.3.11), Chapter II, Melrose (2010) and with Eq. (19) in Melrose (1997a), except for $\dot{t}^{\mu\nu}(\xi)$, because we defined a different coordinate system. Eq. (35) in Paper I offers a similar expression derived in the 3-dimension space with basis $(\tilde{\boldsymbol{e}}_1, \tilde{\boldsymbol{e}}_2, \tilde{\boldsymbol{e}}_3)$. The derivation of Eq. 9 and the related definitions can be found in Appendices A & B.

The 4-vectors in expression (9) can be split into temporal and spatial parts as

$$\mathcal{R}_\mu = (-\omega\xi, \mathrm{R}_j), \quad \mathcal{U}^\mu = (\gamma, \mathrm{u}^j), \quad \mathcal{S}_\mu = (s_0, \mathrm{s}_j). \tag{11}$$

Then the phase becomes $-\imath\mathcal{R}(\xi)\mathcal{U} + \mathcal{S}\mathcal{U} = \imath\omega\xi\cdot\gamma - \imath\mathrm{R}_j\mathrm{u}^j + s_0\gamma + \mathrm{s}_j\mathrm{u}^j = \imath(\omega\xi - \imath s_0)\gamma - \imath(\mathrm{R}_j + \imath\mathrm{s}_j)\mathrm{u}^j$. The momentum integral in the response tensor is

$$\begin{aligned}
&\int \mathrm{d}^3\mathrm{p}\left(-\frac{1}{\gamma}\frac{\mathrm{d}f(\gamma)}{\mathrm{d}\gamma}\mathrm{e}^{\imath(\omega\xi-\imath s_0)\gamma-\imath(\mathrm{R}_j+\imath\mathrm{s}_j)\mathrm{u}^j}\right)\\
&= \int_{|\mathrm{p}|_{\min}}^{|\mathrm{p}|_{\max}} \mathrm{d}|\mathrm{p}|\cdot|\mathrm{p}|^2\cdot\left(-\frac{1}{\gamma}\frac{\mathrm{d}f(\gamma)}{\mathrm{d}\gamma}\right)\cdot\mathrm{e}^{\imath(\omega\xi-is_0)\gamma}\int_0^{2\pi}\int_0^{\pi} e^{-\imath|\mathbf{R}+\imath\mathbf{s}||\mathbf{u}|\cos\theta_\mathrm{p}}\sin\theta_\mathrm{p}\mathrm{d}\theta_\mathrm{p}\mathrm{d}\phi_\mathrm{p}\\
&= I(\xi,\mathcal{S}) - [f(\gamma)\cdot A(\gamma;\xi,\mathcal{S})]_{\gamma_{\min}}^{\gamma_{\max}},
\end{aligned} \tag{12}$$

where

$$I(\xi,\mathcal{S}) = 4\pi\cdot\int_{\gamma_{\min}}^{\gamma_{\max}} f(\gamma)\cdot e^{\imath(\omega\xi-\imath s_0)\gamma}\left[\imath(\omega\xi-\imath s_0)\cdot\frac{\sin\left(|\mathbf{R}+\imath\mathbf{s}|\sqrt{\gamma^2-1}\right)}{|\mathbf{R}+\imath\mathbf{s}|} + \frac{\gamma}{\sqrt{\gamma^2-1}}\cdot\cos\left(|\mathbf{R}+\imath\mathbf{s}|\sqrt{\gamma^2-1}\right)\right]\mathrm{d}\gamma$$

and

$$A(\gamma;\xi,\mathcal{S}) \quad = \quad 4\pi\cdot\frac{\sin(|\mathbf{R}+\imath\mathbf{s}|\sqrt{\gamma^2-1})}{|\mathbf{R}+\imath\mathbf{s}|}\cdot e^{\imath(\omega\xi-\imath s_0)\gamma}.$$

The absolute values are taken as $|\mathbf{R}+\imath\mathbf{s}| = \sqrt{(\mathrm{R}^k+\imath\mathrm{s}^k)(\mathrm{R}_k+\imath\mathrm{s}_k)}$ and $|\mathbf{u}| = \sqrt{\mathrm{u}^k\mathrm{u}_k}$. Note that for any distribution with $f(\gamma_{\min})\cdot A(\gamma_{\min}) \to 0$ and $f(\gamma_{\max})\cdot A(\gamma_{\max}) \to 0$, the second term in last expression of Eq. (12) vanishes.

As the first step of calculation for arbitrary distribution of electrons, we use a δ-function as the distribution

$$f(\gamma) = \delta(\gamma-\gamma_0). \tag{13}$$

Then $I(\xi,\mathcal{S})$ becomes $I(\gamma_0;\xi,\mathcal{S})$ as

$$I(\gamma_0;\xi,\mathcal{S}) = \mathrm{e}^{\imath(\omega\xi-\imath s_0)\gamma_0}\left[\imath(\omega\xi-\imath s_0)\cdot\frac{\sin\left(|\mathbf{R}+\imath\mathbf{s}|p_0\right)}{|\mathbf{R}+\imath\mathbf{s}|} + \frac{\gamma_0}{p_0}\cdot\cos\left(|\mathbf{R}+\imath\mathbf{s}|p_0\right)\right], \tag{14}$$

where

$$p_0 = \sqrt{\gamma_0^2-1} \tag{15}$$

is the dimensionless momentum.

Now we apply the differential operator $\partial^2/(\partial\mathcal{S}_\mu\partial\mathcal{S}_\sigma)$ to $I(\gamma_0;\xi,\mathcal{S})$, set $\mathcal{S}_\mu = 0$, and only choose $(\mu,\nu) = (1,2)$ to isolate the transverse wave component. The final expression of 2×2 response tensor is

$$\alpha^{ij}(k,\gamma_0) \quad = \quad \frac{4\pi e^2}{m_e c}\cdot\imath\int_0^\infty \mathrm{d}(\omega\xi)\cdot\mathrm{e}^{\imath\omega\xi\gamma_0}\left[\dot{t}^{ij}(\xi)\cdot(\imath\omega\xi\Pi_1+\Pi_3) - \widetilde{T}^{ij}(\xi)\cdot(\imath\omega\xi\Pi_2+\Pi_4)\right], \tag{16}$$

where

$$\begin{aligned}
\Pi_1 &= \frac{\sin\left(\mathrm{R}(\xi)p_0\right)}{\mathrm{R}^3(\xi)} - p_0\frac{\cos\left(\mathrm{R}(\xi)p_0\right)}{\mathrm{R}^2(\xi)},\\
\Pi_2 &= \frac{3\sin\left(\mathrm{R}(\xi)p_0\right)}{\mathrm{R}^5(\xi)} - p_0\frac{3\cos\left(\mathrm{R}(\xi)p_0\right)}{\mathrm{R}^4(\xi)} - p_0^2\frac{\sin\left(\mathrm{R}(\xi)p_0\right)}{\mathrm{R}^3(\xi)},\\
\Pi_3 &= \gamma_0\frac{\sin\left(\mathrm{R}(\xi)p_0\right)}{\mathrm{R}(\xi)},\\
\Pi_4 &= \gamma_0\frac{\sin\left(\mathrm{R}(\xi)p_0\right)}{\mathrm{R}^3(\xi)} - \gamma_0 p_0\frac{\cos\left(\mathrm{R}(\xi)p_0\right)}{\mathrm{R}^2(\xi)}
\end{aligned}$$

and

$$\mathrm{R}(\xi) \quad = \quad \sqrt{\mathrm{R}^k(\xi)\mathrm{R}_k(\xi)} \quad = \quad \sqrt{\frac{\omega^2\sin^2\theta}{\Omega_0^2}[2-2\cos(\Omega_0\xi)] + \cos^2\theta\cdot\omega^2\xi^2},$$

$$\tilde{t}^{ij}(\xi) = \begin{pmatrix} \cos(\Omega_0\xi) & -\cos\theta\sin(\Omega_0\xi) \\ \cos\theta\cdot\sin(\Omega_0\xi) & \sin^2\theta+\cos^2\theta\cdot\cos(\Omega_0\xi) \end{pmatrix},$$

$$\widetilde{T}^{ij}(\xi) = \mathrm{R}^i(\xi)\widetilde{\mathrm{R}}^j(\xi) = \frac{\omega^2\sin^2\theta}{\Omega_0^2}\begin{pmatrix} -\left(1-\cos(\Omega_0\xi)\right)^2 & -\cos\theta\left(\sin(\Omega_0\xi)-\Omega_0\xi\right)\left(1-\cos(\Omega_0\xi)\right) \\ \cos\theta\left(\sin(\Omega_0\xi)-\Omega_0\xi\right)\left(1-\cos(\Omega_0\xi)\right) & \cos^2\theta\left(\sin(\Omega_0\xi)-\Omega_0\xi\right)^2 \end{pmatrix}.$$

The differentiation of $A(\gamma;\xi,\mathcal{S})$ yields a response tensor boundary term as

$$\alpha_{\mathrm{B}}^{ij}(k,\gamma_{\min;\max}) = \frac{4\pi e^2}{m_e c}\cdot\imath\int_0^\infty \mathrm{d}(\omega\xi)\mathrm{e}^{\imath\omega\xi\gamma_{\min;\max}}\left[\tilde{t}^{ij}(\xi)\cdot\Pi_1-\widetilde{T}^{ij}(\xi)\cdot\Pi_2\right]. \tag{17}$$

The expression (17) is needed for distributions confined by cut-off Lorentz factors.

The dielectric tensor

$$\varepsilon^{ij} = \delta^{ij}+\frac{4\pi c}{\omega^2}\alpha^{ij} \tag{18}$$

leads to the wave equation

$$\left(\frac{k^2c^2}{\omega^2}\delta^{ij}-\varepsilon^{ij}\right)\begin{pmatrix}\hat{E}_1\\ \hat{E}_2\end{pmatrix} = 0. \tag{19}$$

The corresponding wave dispersion relation is

$$k_\pm^2c^2 = \omega^2+2\pi c\left[\alpha^{11}+\alpha^{22}\pm\sqrt{(\alpha^{11}-\alpha^{22})^2+4\alpha^{12}\alpha^{21}}\right], \tag{20}$$

where $\alpha^{21}=-\alpha^{12}$ due to Onsager principle (Landau & Lifshits 1980) (p. 273). Note that $k_\pm^2$ are real, when α^{ij} only has the Hermitian part, while $k_\pm^2$ become complex, if α^{ij} has both the Hermitian and the anti-Hermitian parts. The approximate relation $k_\pm^2c^2\approx\omega^2+(2\pi c)\mathrm{Re}(\alpha^{11}+\alpha^{22})$ helps to determine if the waves can propagate through medium. For example, the number density $n_e<10^7$ was estimated near Sgr A* (Yuan, Quataert & Narayan 2003), so that $k_\pm$ are dominated by their real parts for $\omega>100$MHz and the waves can propagate.

3 NUMERICAL CALCULATION OF RESPONSE TENSOR AND THE ELLIPTICAL NATURE OF NATURAL MODES

3.1 Numerical calculation of response tensor

We substitute the components of the response tensor from Eq. (16) and perform integration over ξ in complex plane in Mathematica 8. The source code in Mathematica 8 can be found at `http://astroman.org/Faraday_conversion/`. We then find propagation coefficients ρ_V and ρ_Q and absorption coefficients η_I, η_Q, and η_V according to relations (7,8). We analogously compute the boundary terms by substituting the components of α_{B}^{ij} from Eq. (17). Just like in Paper I, we do not perform the integration over ξ along the real axis. To accelerate the convergence we integrate in a complex plane along the ray originating at $\xi=0$ at a positive angle $\psi\in(0,\pi/2)$ to the real axis. Angle ψ needs to be small enough in order to avoid crossing the branch points of α^{ij}. These branch points are produced by zeros of $R(\xi)$. We integrate the full complex expressions to find the response tensor α^{ij} and the boundary term. If γ_0 is small, then computations of anti-Hermitian parts involve substantial cancelations with the values of integrals close to zero. Thus it is hard to reach good accuracy for absorptivity calculations with the method chosen, whereas the correspondent Hermitian parts easily converge. When γ_0 is larger than ~ 10, the values of Hermitian-related part and anti-Hermitian-related part become comparable and all integrals converge.

We choose the fiducial model with $\Omega_0/\omega=10^{-4}$ and $\theta=45^\circ$ and plot on Figure 2 propagation coefficients and absorption coefficients as functions of the Lorentz factor. On the left panel, $2\mathrm{Im}(\alpha^{12})\propto\rho_V$ and $-\mathrm{Re}(\alpha^{11}-\alpha^{22})\propto\rho_Q$, multiplied by $(m_ec)/(4\pi e^2)$, are shown in red and purple dotted lines, respectively. They both monotonically increase as γ_0 increases from 1 to ~ 60. As γ_0 increases further, the profile of ρ_V becomes flatter, while ρ_Q reaches its peak and decreases to negative values.

On the right panel, $\mathrm{Im}(\alpha^{11}-\alpha^{22})\propto\eta_Q$ and $2\mathrm{Re}(\alpha^{12})\propto\eta_V$, divided by $(4\pi e^2/m_ec)$, are shown in green and blue dotted lines, respectively. We also show $(\omega/2\pi)\eta_Q'$ and $(\omega/2\pi)\eta_V'$ as long-dashed and dashed black lines, respectively. Here η_Q' and η_V' corresponds to the integrals in Sazonov (1969)[1]

$$\begin{aligned}\eta_Q' &= -\frac{\nu_B\sin\theta}{\nu}\frac{\sqrt{3}e^2}{4m_ec\nu}\int_1^\infty \mathrm{d}\gamma\cdot\gamma^2\frac{\partial}{\partial\gamma}\left[\frac{\delta(\gamma-\gamma_0)}{\gamma^2}\right]\frac{\nu}{\nu_\gamma}K_{2/3}\left(\frac{\nu}{\nu_\gamma}\right)\\ \eta_V' &= -\frac{\nu_B\cos\theta}{\nu}\frac{e^2}{\sqrt{3}m_ec\nu}\int_1^\infty \mathrm{d}\gamma\cdot\gamma\frac{\partial}{\partial\gamma}\left[\frac{\delta(\gamma-\gamma_0)}{\gamma^2}\right]\left[\frac{\nu}{\nu_\gamma}K_{1/3}\left(\frac{\nu}{\nu_\gamma}\right)+\int_{\nu/\nu_\gamma}^\infty \mathrm{d}zK_{1/3}(z)\right],\end{aligned} \tag{21}$$

---

[1] The sign of η_V is opposite to that in Sazonov (1969), if the current IAU/IEEE definition of the sign of circular polarization is followed.

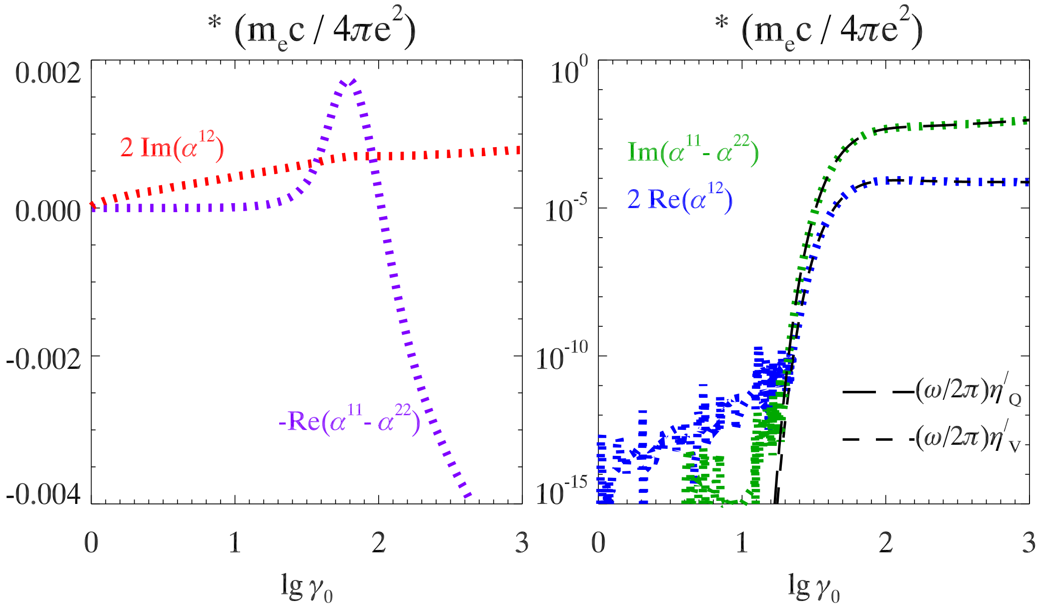

Figure 2. Absorption and propagation coefficients for the fiducial model with parameters $\Omega_0/\omega = 10^{-4}$ and $\theta = 45°$ for the monoenergetic electron distribution. *Left*: $2\mathrm{Im}(\alpha^{12}) \propto \rho_V$ (Faraday rotation, in red) and $-\mathrm{Re}(\alpha^{11} - \alpha^{22}) \propto \rho_Q$ (Faraday conversion, in purple). *Right*: $\mathrm{Im}(\alpha^{11} - \alpha^{22}) \propto \eta_Q$ (absorption of linearly-polarized waves, green) and $2\mathrm{Re}(\alpha^{12}) \propto \eta_V$ (absorption of circularly-polarized waves, blue). Approximate absorption coefficients based on Sazonov (1969), in particular, $(\omega/2\pi)\eta'_Q$ and $(\omega/2\pi)\eta'_V$, are shown in long-dashed and dashed black lines, respectively.

where ν_B is the cyclotron frequency, $\nu_\gamma = (3eB\sin\theta\gamma^2)/(4\pi m_e c)$ is the characteristic frequency, and K_α is the modified Bessel function of the second kind of order α. We integrate by parts to deal with the differential of the δ-function. Note that our absorptivities deviate a lot from the correct values, when γ_0 is small. As mentioned earlier, this is due to large cancelations of the parts of the integral, so that absorptivities cannot easily converge. When $\gamma_0 > 30$, they coincide with the approximate expressions.

Despite inaccuracy at low Lorentz factors, the calculation clearly shows an important property of plasma absorption. The absorption in Q-component is smaller, compared to that in V-component $\eta_Q < |\eta_V|$ at low Lorentz factors, while $\eta_Q > |\eta_V|$ at high Lorentz factors. This shows that the radiation mechanism changes from CP-dominated cyclotron to LP-dominated synchrotron as the Lorentz factor increases. The traditional approximations do not exhibit this property, because they assume high Lorentz factors.

3.2 The axial radios and natural modes

The corresponding eigenvectors from the wave equation are $(\widetilde{T}^+, \imath)^{\mathrm{T}}$ and $(\widetilde{T}^-, \imath)^{\mathrm{T}}$, respectively, where

$$\begin{aligned}
\widetilde{T}^+ &= \frac{\alpha^{11} - \alpha^{22} + \sqrt{(\alpha^{11} - \alpha^{22})^2 + 4\alpha^{12}\alpha^{21}}}{2\imath\alpha^{12}}, \\
\widetilde{T}^- &= \frac{\alpha^{11} - \alpha^{22} - \sqrt{(\alpha^{11} - \alpha^{22})^2 + 4\alpha^{12}\alpha^{21}}}{2\imath\alpha^{12}}.
\end{aligned} \tag{22}$$

These $\widetilde{T}^+$ and $\widetilde{T}^-$ are complex axial ratios of the transverse wave. They obey the relation

$$\widetilde{T}^+\widetilde{T}^- = -1. \tag{23}$$

The polar decomposition into real amplitudes $T^\pm (\geqslant 0)$ and phases $\varphi^\pm$ reads

$$\widetilde{T}^+ = T^+ \mathrm{e}^{\imath\varphi^+} \quad \text{and} \quad \widetilde{T}^- = T^- \mathrm{e}^{\imath\varphi^-}, \tag{24}$$

so that

$$T^+T^- = 1 \quad \text{and} \quad \varphi^+ + \varphi^- = -\pi. \tag{25}$$

These two wave eigenvalues define two natural wave modes as

$$
\begin{aligned}
\hat{\boldsymbol{E}}_{+} &= \frac{\widetilde{T}^{+}\hat{\boldsymbol{E}}_1 + \imath\hat{\boldsymbol{E}}_2}{\sqrt{1+\widetilde{T}^{+}\cdot conj[\widetilde{T}^{+}]}} &= \frac{T^{+}\mathrm{e}^{\imath\varphi^{+}}\hat{\boldsymbol{E}}_1 + \imath\hat{\boldsymbol{E}}_2}{\sqrt{1+(T^{+})^2}} \\
\hat{\boldsymbol{E}}_{-} &= \frac{\widetilde{T}^{-}\hat{\boldsymbol{E}}_1 + \imath\hat{\boldsymbol{E}}_2}{\sqrt{1+\widetilde{T}^{-}\cdot conj[\widetilde{T}^{-}]}} &= \frac{T^{-}\mathrm{e}^{\imath\varphi^{-}}\hat{\boldsymbol{E}}_1 + \imath\hat{\boldsymbol{E}}_2}{\sqrt{1+(T^{-})^2}}
\end{aligned}
\tag{26}
$$

In practise, $\varphi^{+} < -\pi/2$ and $\varphi^{-} > -\pi/2$. Thus, the electric vector $\hat{\boldsymbol{E}}_{+}$ rotates counter-clockwise and the electric vector $\hat{\boldsymbol{E}}_{-}$ clockwise, as seen by the observer. Note that

$$
\hat{\boldsymbol{E}}_{+}\cdot conj[\hat{\boldsymbol{E}}_{-}] = \frac{\mathrm{e}^{\imath(\varphi^{+}-\varphi^{-})}+1}{T^{+}+T^{-}} \quad \begin{cases} = 0, & \text{iff} \quad \varphi^{+} = -\pi \\ \neq 0, & \text{otherwise} \end{cases}
\tag{27}
$$

That is $\hat{\boldsymbol{E}}_{+}$ and $\hat{\boldsymbol{E}}_{-}$ are not perpendicular to each other, unless the anti-Hermitian part, absorption, can be neglected.

3.3 Properties of radiation in natural modes

Let us decompose the natural modes along $\hat{\boldsymbol{E}}_1$ and $\hat{\boldsymbol{E}}_2$ as

$$
\boldsymbol{E}_1^{\pm} = \frac{A^{\pm}T^{\pm}\mathrm{e}^{\imath\varphi^{+}}}{\sqrt{1+(T^{\pm})^2}}\hat{\boldsymbol{E}}_1 \quad \text{and} \quad \boldsymbol{E}_2^{\pm} = \frac{\imath A^{\pm}}{\sqrt{1+(T^{\pm})^2}}\hat{\boldsymbol{E}}_2
\tag{28}
$$

We define the Stokes parameters for natural modes as

$$
\begin{aligned}
I_0^{\pm} &= <\boldsymbol{E}_1^{\pm}\cdot conj[\boldsymbol{E}_1^{\pm}]> + <\boldsymbol{E}_2^{\pm}\cdot conj[\boldsymbol{E}_2^{\pm}]> = \left(A^{\pm}\right)^2, \\
Q_0^{\pm} &= <\boldsymbol{E}_1^{\pm}\cdot conj[\boldsymbol{E}_1^{\pm}]> - <\boldsymbol{E}_2^{\pm}\cdot conj[\boldsymbol{E}_2^{\pm}]> = \left(A^{\pm}\right)^2\cdot\frac{\left(T^{\pm}\right)^2-1}{1+(T^{\pm})^2}, \\
U_0^{\pm} &= <\boldsymbol{E}_1^{\pm}\cdot conj[\boldsymbol{E}_2^{\pm}]> + <\boldsymbol{E}_2^{\pm}\cdot conj[\boldsymbol{E}_1^{\pm}]> = \left(A^{\pm}\right)^2\cdot\frac{2T^{\pm}\sin\varphi^{\pm}}{1+(T^{\pm})^2}, \\
V_0^{\pm} &= \imath\left(<\boldsymbol{E}_1^{\pm}\cdot conj[\boldsymbol{E}_2^{\pm}]> - <\boldsymbol{E}_2^{\pm}\cdot conj[\boldsymbol{E}_1^{\pm}]>\right) = \left(A^{\pm}\right)^2\cdot\frac{2T^{\pm}\cos\varphi^{\pm}}{1+(T^{\pm})^2}.
\end{aligned}
\tag{29}
$$

Note that $X_0 \neq X_0^{+} + X_0^{-}, (X_0 = I_0, Q_0, U_0, V_0)$, since $< \hat{\boldsymbol{E}}_{+}\cdot conj[\hat{\boldsymbol{E}}_{-}] > \neq 0$ unless $\varphi^{+} = -\pi$. These Stokes parameters correspond to elliptically polarized radiation with ellipticity β

$$
\beta^{\pm} = \frac{1}{2}\sin^{-1}\frac{V_0^{\pm}}{I_0^{\pm}} = \frac{1}{2}\sin^{-1}\left(\frac{2T^{\pm}\cos\varphi^{\pm}}{1+(T^{\pm})^2}\right)
\tag{30}
$$

and the electric vector position angle (EVPA)

$$
\chi^{\pm} = \frac{1}{2}\tan^{-1}\frac{U_0^{\pm}}{Q_0^{\pm}} = \frac{1}{2}\tan^{-1}\left(\frac{2T^{\pm}\sin\varphi^{\pm}}{(T^{\pm})^2-1}\right).
\tag{31}
$$

The relations between the axial ratios and the Stokes parameters for each mode are

$$
\frac{\left(R_{\mathrm{CP}}^{+}\right)^2}{\left(R_{\mathrm{LP}}^{+}\right)^2}\left(=\frac{\left(V_0^{+}\right)^2}{\left(Q_0^{+}\right)^2+\left(U_0^{+}\right)^2}\right) = \frac{\left(R_{\mathrm{CP}}^{-}\right)^2}{\left(R_{\mathrm{LP}}^{-}\right)^2}\left(=\frac{\left(V_0^{-}\right)^2}{\left(Q_0^{-}\right)^2+\left(U_0^{-}\right)^2}\right) = \left(\frac{2}{|\widetilde{T}^{+}+\widetilde{T}^{-}|}\right)^2 |\mathrm{Re}(\widetilde{T}^{+})\mathrm{Re}(\widetilde{T}^{-})|.
\tag{32}
$$

We define a special quantity

$$
Z^{\pm} = \frac{R_{\mathrm{CP}}^{\pm}}{R_{\mathrm{LP}}^{\pm}}\cdot\frac{\rho_Q}{\rho_V},
\tag{33}
$$

which effectively measures how well the normal modes can be described, if we ignore absorption. We show amplitudes $T^{\pm}(\geqslant 0)$, phases $\varphi^{\pm}$, ellipticities $\beta^{\pm}$, and EVPA $\chi^{\pm}$ on Figure 3. All quantities with superscript $(^{+})$ are drawn in solid lines and those with $(^{-})$ are dashed.

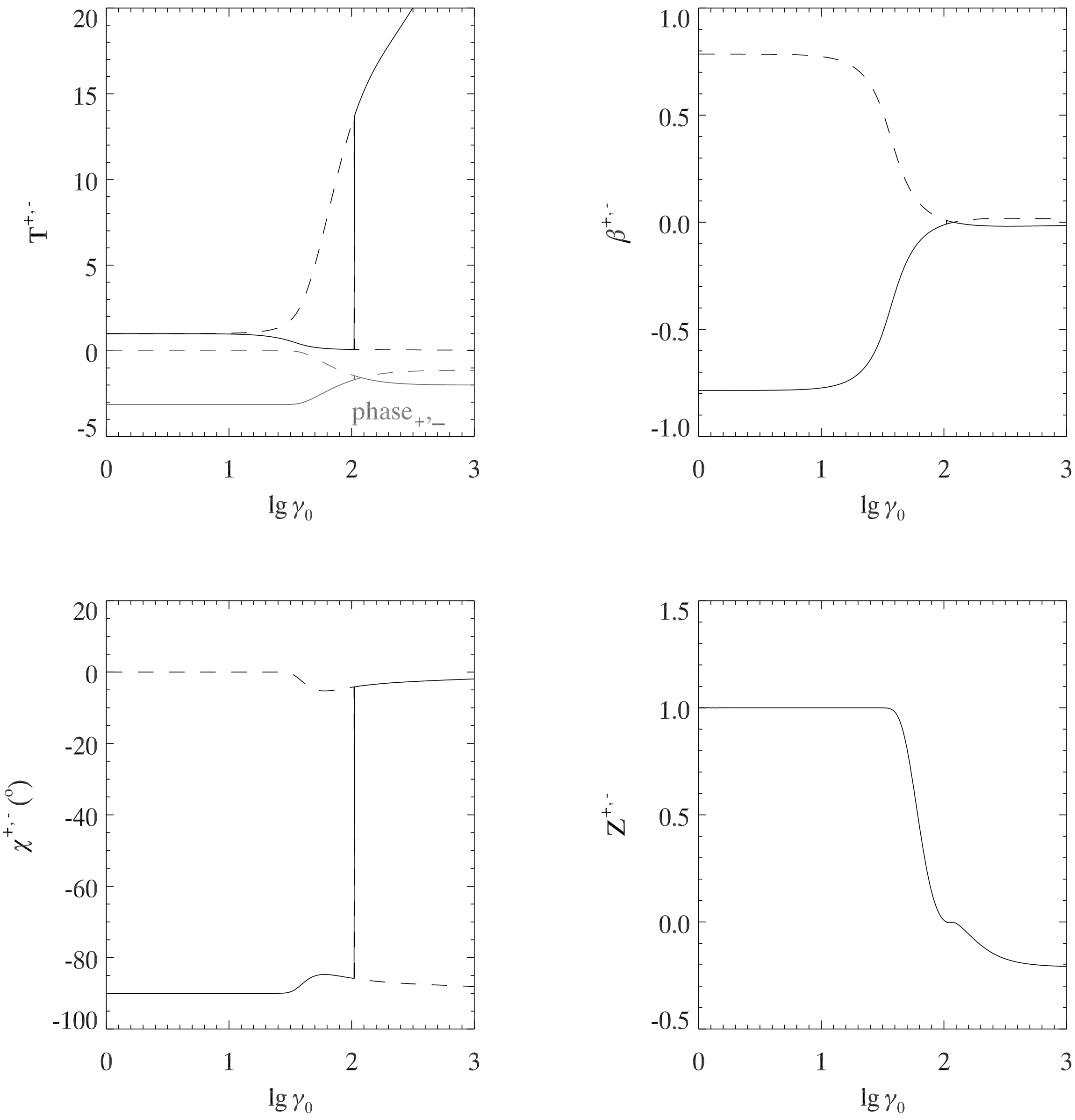

Figure 3. Properties of two natural modes for the monoenergetic particle distribution. Amplitudes $T^{\pm}$ (black) and phases $\varphi^{\pm}$ (grey) of complex axial ratio, ellipticity $\beta^{\pm}$ ($\sim \pm\pi/4$ corresponding to circular polarized waves and ~ 0 to linear ones), EVPA $\chi^{\pm}$, and $Z^{+} = Z^{-}$ (eq. 33) are shown in four panels, respectively. Lines for ($^{+}$)-mode are solid and for ($^{-}$)-mode are dashed.

3.3.1 Cold plasma limit

In cold plasma the anti-Hermitian part of the response tensor can be neglected compared to the Hermitian part. In this case, $\varphi^{+} = -\pi$, $\varphi^{-} = 0$ (see grey lines on the top left panel of Figure 3), $U_0^{+} = U_0^{-} = 0$, and $|\rho_V| >> |\rho_Q|$. The axial ratios are

$$\begin{aligned} \widetilde{T}^{+} &= \frac{1-\sqrt{1+(\rho_V/\rho_Q)^2}}{\rho_V/\rho_Q} &= -T^{+} &\approx -1, \\ \widetilde{T}^{-} &= \frac{1+\sqrt{1+(\rho_V/\rho_Q)^2}}{\rho_V/\rho_Q} &= T^{-} &\approx 1. \end{aligned} \tag{34}$$

They are consistent with the Eq.(4.6) in Melrose (1997b). The corresponding ellipticity β and EVPAs are

$$\beta^{+} = -\beta^{-} = \frac{1}{2}\sin^{-1}\left(-\frac{2}{T^{+}+T^{-}}\right) \approx -\frac{\pi}{4},$$

$$\chi^{+} = -\frac{\pi}{2}, \quad \chi^{-} = 0. \tag{35}$$

Two natural modes are circularly polarized. They are orthogonal with major and minor axes aligned with $\boldsymbol{e}_1$ and $\boldsymbol{e}_2$, respectively. The relation between the Stokes parameters and the axial ratios becomes

$$\frac{R^{\pm}_{\rm CP}}{R^{\pm}_{\rm LP}} = \frac{R_{\rm CP}}{R_{\rm LP}} = \frac{V_0}{Q_0} = \frac{2}{T^{+} - T^{-}} = \frac{\rho_V}{\rho_Q}, \quad \text{i.e.,} \quad Z^{\pm} = 1. \tag{36}$$

This means the ratio of circular to linear radiation intensities in cold plasma eigenmodes equals the ratio of Faraday rotation to Faraday conversion coefficients. The total emission is dispersionless in a sense that the term $(\vec{\rho} \times \vec{p})$ in transfer of polarized radiation in Landi Degl'Innocenti & Landolfi (2004) vanishes, also see Huang et al. (2009) for similar results with different definitions of the axial ratios. As Faraday rotation is much stronger than Faraday conversion, then the circular polarized intensity is much larger than the linear polarized intensity in eigenmodes. These are the well-known properties of 'cyclotron'/cold plasma regime.

In the limit $\omega^2 >> \alpha^{\mu\nu}$, the refractive indices of two modes are

$$n_{\pm} = \frac{k_{\pm} c}{\omega} = \sqrt{1 + \frac{2\pi c}{\omega^2}(\alpha^{11} + \alpha^{22} \pm \frac{\omega}{2\pi}\rho_V)} \approx 1 + \frac{1}{2}\frac{2\pi c}{\omega^2}(\alpha^{11} + \alpha^{22} \pm \frac{\omega}{2\pi}\rho_V), \tag{37}$$

which corresponds to standard rotation by θ_f of EVPA plane, Faraday rotation effect, as

$$\frac{{\rm d}\theta_f}{{\rm d}l} = \frac{\omega}{2c}(n_{+} - n_{-}) \approx \frac{1}{2}\rho_V \tag{38}$$

3.3.2 Ultrarelativistic plasma limit

In plasma with very high Lorentz factors ρ_Q changes its sign to the negative. Two natural modes also change their polarization property from circular to linear. We find an interesting result that the quantity $Z^{\pm}$ is approaching another constant. This means the proportion of linear to circular radiation in each eigenmode can still be easily measured by the proportion of Faraday conversion to rotation.

As it appears $\eta_Q \approx -2\rho_Q$ in this limit, and $|\eta_V| << |\rho_V| << |\rho_Q|$. So the complex axial ratios become

$$\begin{aligned} \widetilde{T}^{\pm} &= \frac{\rho_Q}{\rho_V} \frac{-1 + \imath\left(\frac{\eta_Q}{\rho_Q}\right) \mp \sqrt{\left[-1 + \imath\left(\frac{\eta_Q}{\rho_Q}\right)\right]^2 - \left[\left(\frac{\eta_V}{\rho_Q}\right) + \imath\left(\frac{\rho_V}{\rho_Q}\right)\right]^2}}{\imath\left[\left(\frac{\eta_V}{\rho_V}\right) + \imath\right]} \\ &\approx \frac{\rho_Q}{\rho_V}\left[1 + 2\imath \pm \sqrt{(1+2\imath)^2 + (\rho_V/\rho_Q)^2}\right] \approx \frac{\rho_Q}{\rho_V}\left[1 + 2\imath \pm (1+2\imath)\left(1 + \frac{1}{2}\left(\frac{\rho_V/\rho_Q}{1+2\imath}\right)^2\right)\right]. \end{aligned} \tag{39}$$

We derive

$$\begin{aligned} \widetilde{T}^{+} &\to \frac{\rho_Q}{\rho_V} \cdot (2 + 4\imath), \quad T^{+} \to \infty, \quad \varphi^{+} \to -\pi + \tan^{-1}(2) \approx -2, \\ \widetilde{T}^{-} &\to -\frac{\rho_V}{\rho_Q} \cdot (0.1 - 0.2\imath), \quad T^{-} \to 0, \quad \varphi^{-} = -\pi - \varphi^{+} \to -\tan^{-1}(2) \approx -1, \\ \beta^{\pm} &\to 0, \quad \chi^{+} \to 0, \quad \chi^{-} \to -\frac{\pi}{2}, \end{aligned} \tag{40}$$

and

$$\begin{aligned} \frac{R^{+}_{\rm CP}}{R^{+}_{\rm LP}} &= \frac{R^{-}_{\rm CP}}{R^{-}_{\rm LP}} = \frac{2}{|\widetilde{T}^{+} + \widetilde{T}^{-}|}\sqrt{|{\rm Re}(\widetilde{T}^{+}){\rm Re}(\widetilde{T}^{-})|} \to \frac{2}{4.47 \cdot |\rho_Q/\rho_V|}\sqrt{2\frac{\rho_Q}{\rho_V} \cdot 0.1\frac{\rho_V}{\rho_Q}} \approx -0.2 \cdot \frac{\rho_V}{\rho_Q} \\ \text{i.e.,} \quad Z^{\pm} &\to -0.2 \end{aligned} \tag{41}$$

Note that the total intensity cannot be calculated by simply adding intensities in two modes, because they are not orthogonal.

3.3.3 Intermediate regime

In plasma with intermediate Lorentz factors (about $\gamma_0 \sim 10^{1-2}$ for the fiducial model with $\Omega_0/\omega = 10^{-4}$), the properties of the natural modes change gradually from those in cold limit to those in ultra-relativistic limit.

As γ_0 increases, T^{+} decreases to 0, while T^{-} approaches ∞, ellipticities $|\beta^{\pm}|$ decrease to 0, EVPAs $\chi^{\pm}$ deviate from $-90°$ (or $0°$). At a special value of γ_0^{*} the Faraday conversion coefficient $-{\rm Re}(\alpha^{11} - \alpha^{22})$ changes its sign, as shown in Figure 2. The Lorentz factor for the fiducial model is $\gamma_0^{*} \approx 100$. Flips of $T^{\pm}$, $\beta^{\pm}$, and $\chi^{\pm}$ between two modes help to preserve the handedness of the modes. That is the wave with $\hat{\boldsymbol{E}}_{+}$ always has a counter-clockwise rotation, while the wave described by $\hat{\boldsymbol{E}}_{-}$ has a clockwise one. The value of $Z^{\pm}$ decreases in the intermediate regime from 1 to ~ -0.2.

4 PROPAGATION AND ABSORPTION COEFFICIENTS FOR ISOTROPIC PLASMAS WITH ARBITRARY ENERGY DISTRIBUTIONS

4.1 Integration over particle distribution function

The final form of the response tensor is related to $I(\xi,\mathcal{S})$ as shown by Eq. (12). With the aid of

$$I(\xi,\mathcal{S}) \quad = \quad \int f(\gamma) I(\gamma_0;\xi,\mathcal{S})\mathrm{d}\gamma, \tag{42}$$

one has

$$\begin{aligned}\alpha^{ij}(k) \quad &= \quad \left\{\frac{\imath e^2\omega}{m_e c}\int_0^{\infty}\mathrm{d}\xi t^{\nu}_{\sigma}(-\xi)\left[\frac{\partial^2}{\partial\mathcal{S}_\mu\partial\mathcal{S}_\sigma}I(\xi,\mathcal{S}) - \left(f(\gamma)\cdot\frac{\partial^2}{\partial\mathcal{S}_\mu\partial\mathcal{S}_\sigma}A(\gamma;\xi,\mathcal{S})\right)\Bigg|_{\gamma_{\min}}^{\gamma_{\max}}\right]_{s_\mu=0}\right\}_{\mu,\nu=1,2} \\ &= \quad \int_{\gamma_{\min}}^{\gamma^{\max}} f(\gamma)\cdot\alpha^{ij}(k,\gamma)\mathrm{d}\gamma - f(\gamma_{\max})\cdot\alpha^{ij}_{\mathrm{B}}(k,\gamma_{\max}) + f(\gamma_{\min})\cdot\alpha^{ij}_{\mathrm{B}}(k,\gamma_{\min}).\end{aligned} \tag{43}$$

The isotropic distribution function $f(\gamma)$ is normalized as $\int f(\gamma)\mathrm{d}^3\mathrm{p} = n_e$. In this section we compute the propagation and absorption coefficients for thermal and power-law particle distributions.

4.1.1 Thermal distribution

The thermal distribution is

$$f(\gamma) \quad = \quad \frac{n_e}{4\pi\Theta_e K_2(\Theta_e^{-1})}\mathrm{e}^{-\gamma/\Theta_e}, \quad 1 \leqslant \gamma < +\infty, \tag{44}$$

where $\Theta_e = \mathrm{k_B}T_e/(m_e c^2)$ is the dimensionless particle temperature. It is normalized to number density of electrons n_e as

$$\int f(\gamma)\mathrm{d}^3\mathrm{p} = 4\pi\int_1^{+\infty}\gamma\sqrt{\gamma^2-1}f(\gamma)\mathrm{d}\gamma = n_e. \tag{45}$$

In this case, $f(\gamma_{\max}\to+\infty)\to 0$, so that the response tensor becomes

$$\alpha^{ij}(k) = \frac{n_e}{4\pi\Theta_e K_2(\Theta_e^{-1})}\left[\int_1^{+\infty}\mathrm{e}^{-\gamma/\Theta_e}\cdot\alpha^{ij}(k,\gamma)\mathrm{d}\gamma + \mathrm{e}^{-1/\Theta_e}\cdot\alpha^{ij}_{\mathrm{B}}(k,1)\right] = \frac{n_e}{4\pi\Theta_e K_2(\Theta_e^{-1})}\int_1^{+\infty}\mathrm{e}^{-\gamma/\Theta_e}\cdot\alpha^{ij}(k,\gamma)\mathrm{d}\gamma, \tag{46}$$

since $\alpha^{ij}_{\mathrm{B}}(k,1)\to 0$. The propagation and absorption coefficients for $n_e = 1$ are shown in thick dotted lines on Figure 4.

On the left panel we show in dashed grey lines the linear approximations to propagation coefficients elaborated in Melrose (1997b); Shcherbakov (2008) for $n_e = 1$. The related formulae are[2]

$$\begin{aligned}\rho_{Q,\mathrm{lin}} \quad &= \quad \frac{2\pi e^2\Omega_0^2}{m_e c\cdot\omega^3}\left(\frac{K_1(\Theta_e^{-1})}{K_2(\Theta_e^{-1})}\sin^2\theta + 6\Theta_e\sin^2\theta\right), \\ \rho_{V,\mathrm{lin}} \quad &= \quad \frac{4\pi e^2\Omega_0}{m_e c\cdot\omega^2}\frac{K_0(\Theta_e^{-1})}{K_2(\Theta_e^{-1})}\cos\theta.\end{aligned} \tag{47}$$

We scale $2\mathrm{Im}(\alpha^{12})$ and $(\omega/2\pi)\rho_{V,\mathrm{lin}}$ by a factor of 300 for a better layout together with $\mathrm{Re}(\alpha^{11}-\alpha^{22})$ and $(\omega/2\pi)\rho_{Q,\mathrm{lin}}$. Note that $\rho_{V,\mathrm{lin}}$ is a good approximation for Faraday rotation coefficient at any temperature, while $\rho_{Q,\mathrm{lin}}$ is a good approximation for Faraday conversion coefficient only at low temperatures, not at high temperatures. The peak of Faraday conversion for monoenergetic particles leads to a similar peak at about 10^{11}K for thermal distribution. Faraday conversion is much lower than the linear approximation predicts, if the temperature rises. We will show in the last section that the linear approximations lead to wrong predictions of circular polarization from Sgr A*, the difference being a factor of several.

Black long-dashed and dashed lines on the right panel show $(\omega/2\pi)\eta'_Q$ and $(\omega/2\pi)\eta'_V$, for $n_e = 1$, respectively. The absorption coefficients η'_Q and η'_V are calculated according to Eq. (21) by substituting the thermal distribution function. Similar to the case of monoenergetic particles, our thermal calculations match the approximations well at high temperatures, while they become inaccurate in low temperatures. In practice one can just adopt the simple traditional approximations for synchrotron absorption coefficients.

We show $T^{\pm}$ and phases, $\beta^{\pm}$, $\chi^{\pm}$, and $Z^{\pm}$ on Figure 5. In general, they are similar to those for δ-function distribution discussed in § 3.3. Note that EVPA (χ) deviates by as much as $\sim 20^\circ$ from 0° (or -90°) at $T_e \approx 10^{11}$K.

---

[2] Note, that Faraday conversion coefficient in the "linear" regime is actually proportional to $(\Omega_0/\omega)^2$.

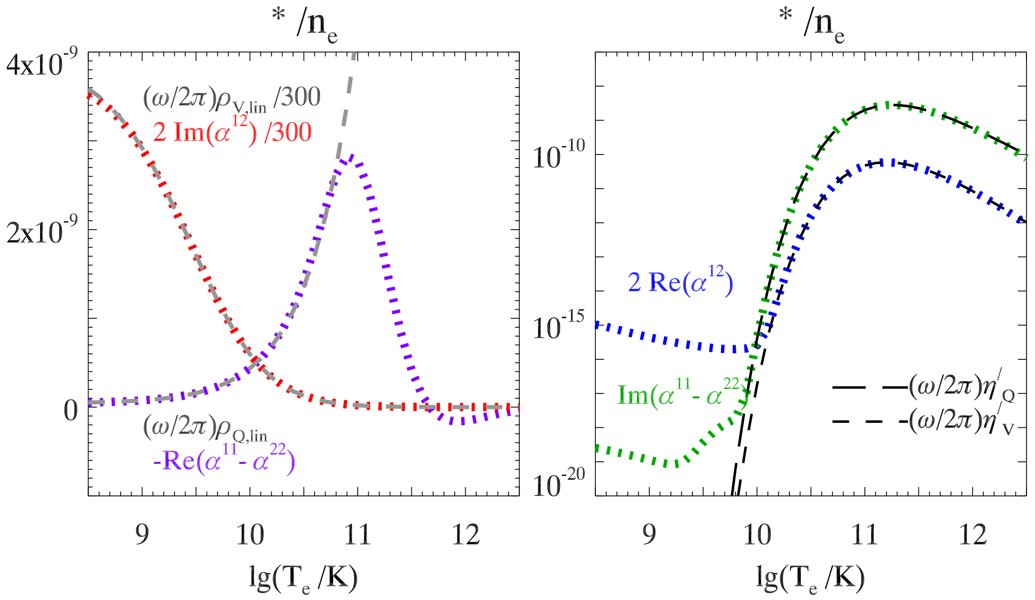

Figure 4. Propagation and absorption coefficients for thermal energy distribution. *Left*: Faraday rotation and conversion. Linear approximations by Melrose (1997b) are shown in black dashed lines. *Right*: Absorption coefficients. Traditional approximations are shown in black solid lines.

4.1.2 Power-law distribution

Number density per unit Lorentz factor is

$$N(\gamma) \quad = \quad \frac{b-1}{\gamma_{\rm min}^{1-b}-\gamma_{\rm max}^{1-b}}\cdot n_e\gamma^{-b}, \qquad \gamma_{\rm min}<\gamma<\gamma_{\rm max}, b>1 \tag{48}$$

for power-law particle distribution, where b is the energy-spectral index, set greater than 1 as examples. Thus the distribution function is

$$f(\gamma)=\frac{N(\gamma)}{4\pi\gamma^2|{\rm v}|} \quad = \quad \frac{n_e}{4\pi}\cdot\frac{b-1}{\gamma_{\rm min}^{1-b}-\gamma_{\rm max}^{1-b}}\cdot\frac{\gamma^{-(b+1)}}{\sqrt{\gamma^2-1}}, \qquad \gamma_{\rm min}<\gamma<\gamma_{\rm max}. \tag{49}$$

We set $\gamma_{\rm max}=+\infty$ in computations below for $b>1$. Then $f(\gamma_{\rm max}\to+\infty)\to 0$, and the response tensor becomes

$$\alpha^{ij}(k)=\frac{n_e(b-1)}{4\pi\gamma_{\rm min}^{1-b}}\left[\int_{\gamma_{\rm min}}^{+\infty}\frac{\gamma^{-b}}{\sqrt{\gamma^2-1}}\cdot\alpha^{ij}(k,\gamma){\rm d}\gamma+\frac{\gamma_{\rm min}^{-b}}{\sqrt{\gamma_{\rm min}^2-1}}\cdot\alpha_{\rm B}^{ij}(k,\gamma_{\rm min})\right]. \tag{50}$$

We show the results of numerical integration for $b=2.5$ on Figure 6. On the left panel, we also show approximations for propagation coefficients given by Sazonov (1969) for $n_e=1$ in dashed grey lines. The related formulae are

$$\begin{aligned}\rho_{Q,{\rm appr}} \quad &= \quad 8.5\times10^{-3}\cdot\frac{2}{(b-2)}\left[\left(\frac{\omega}{\Omega_0\sin\theta\gamma_{\rm min}^2}\right)^{(b-2)/2}-1\right]\frac{(b-1)}{\gamma_{\rm min}^{1-b}}\cdot\left(\frac{\Omega_0}{\omega}\sin\theta\right)^{(b+2)/2}\cdot\frac{2\pi}{\omega},\\ \rho_{V,{\rm appr}} \quad &= \quad 1.7\times10^{-2}\cdot\frac{\ln\gamma_{\rm min}}{(b+1)\gamma_{\rm min}^{b+1}}\cdot\frac{(b-1)}{\gamma_{\rm min}^{1-b}}\cdot\frac{\Omega_0}{\omega}\cos\theta\cdot\frac{2\pi}{\omega}.\end{aligned} \tag{51}$$

(Similar formulae can be also found in Jones & O'Dell (1977).)

We scale $2{\rm Im}(\alpha^{12})$ and $(\omega/2\pi)\rho_{V,{\rm appr}}$ by a factor of 150 for a better layout. Here $\rho_{V,{\rm appr}}$ is a good approximation of Faraday rotation coefficient only for large $\gamma_{\rm min}$. It significantly underestimates Faraday rotation, if the cut-off Lorentz factor is low. The approximation $\rho_{Q,{\rm appr}}$ works well for Faraday conversion coefficient, if $\gamma_{\rm min}<100$. It accurately describes the exact behavior including the peak.

On the right panel of Figure 6 long-dashed and dashed black lines show $(\omega/2\pi)\eta'_Q$ and $(\omega/2\pi)\eta'_V$ respectively for $n_e=1$. The approximate absorption coefficients η'_Q and η'_V are computed based on Eq. 21 by substituting the power-law distribution function. In this case our calculation of ${\rm Im}(\alpha^{11}-\alpha^{22})$ and $2{\rm Re}(\alpha^{12})$ match their traditional approximations well for all $\gamma_{\rm min}$. This is because the particles with high γ play a large role in power-law distribution compared to the thermal, so that the inaccuracy at low γ's is concealed. Similar to the case of thermal distribution, one can adopt simple traditional approximations

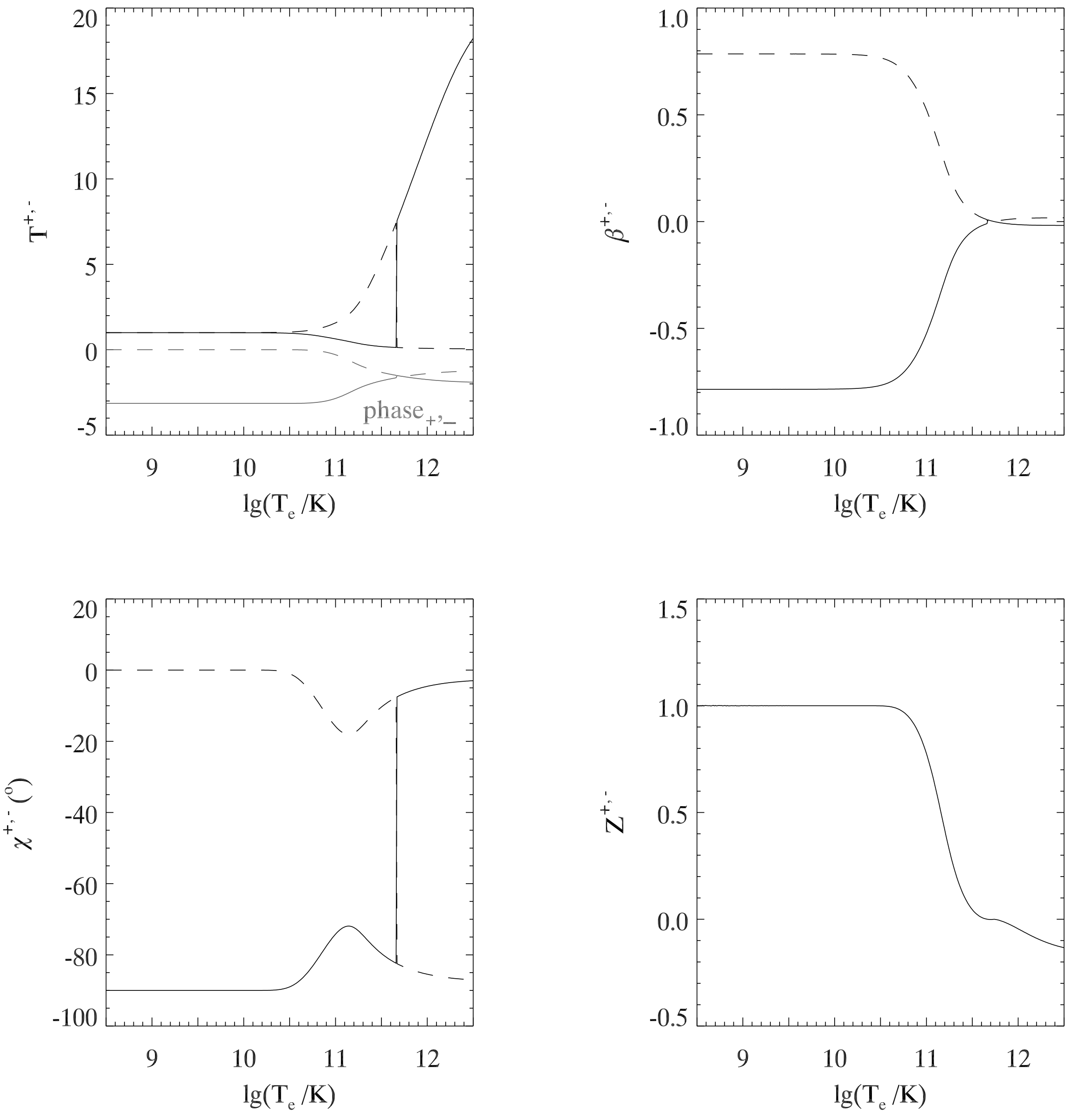

Figure 5. Properties of two natural modes in plasma with thermal energy distribution.. Amplitudes $T^{\pm}$ (black) and phases $\varphi^{\pm}$ (grey) of complex axial ratio, ellipticity $\beta^{\pm}$, EVPA $\chi^{\pm}$, and $Z^{+}=Z^{-}$ (eq. 33) are shown on four panels, respectively.

for synchrotron absorption. We also show approximations for absorption coefficients given by Sazonov (1969) for $n_e = 1$, in long-dashed and dashed grey lines. The corresponding expressions are

$$\begin{aligned}\eta_{Q,\rm appr} &= 3.1\times10^{-4}\cdot(b+2)\,\Gamma\left(\frac{3b+2}{12}\right)\Gamma\left(\frac{3b+10}{12}\right)\frac{(b-1)}{\gamma_{\rm min}^{1-b}}\cdot\left(3\frac{\Omega_0}{\omega}\sin\theta\right)^{(b+2)/2}\cdot\frac{2\pi}{\omega},\\ \eta_{V,\rm appr} &= 4.1\times10^{-4}\cdot\frac{b+3}{b+1}\Gamma\left(\frac{3b+7}{12}\right)\Gamma\left(\frac{3b+11}{12}\right)\frac{(b-1)}{\gamma_{\rm min}^{1-b}}\cdot(b+2)\cot\theta\left(3\frac{\Omega_0}{\omega}\sin\theta\right)^{(b+3)/2}\cdot\frac{2\pi}{\omega}.\end{aligned}\tag{52}$$

These approximations are good for $\gamma_{\rm min} < 100$, while they overestimate the absorption at larger $\gamma_{\rm min}$.

We show $T^{\pm}$ and phases, $\beta^{\pm}$, $\chi^{\pm}$, and $Z^{\pm}$ in black and grey on Figure 7 for power-law particle distribution with $b = 2.5$. The same quantities for power-law distribution with $b = 1.5$ are shown in green and cyan for comparison. The plots are similar to those for monoenergetic distribution or thermal distribution. The curves for $b = 1.5$ and $b = 2.5$ almost coincide for high $\gamma_{\rm min}$. At low $\gamma_{\rm min}$, however, $\chi^{\pm}$ deviate more from $-90°$ (or $0°$) at $b = 1.5$ compared to the case with $b = 2.5$, and $Z^{\pm} \neq 1$ for $b = 1.5$. This is because the particles with high Lorentz factors affect the results more for a lower spectral index.

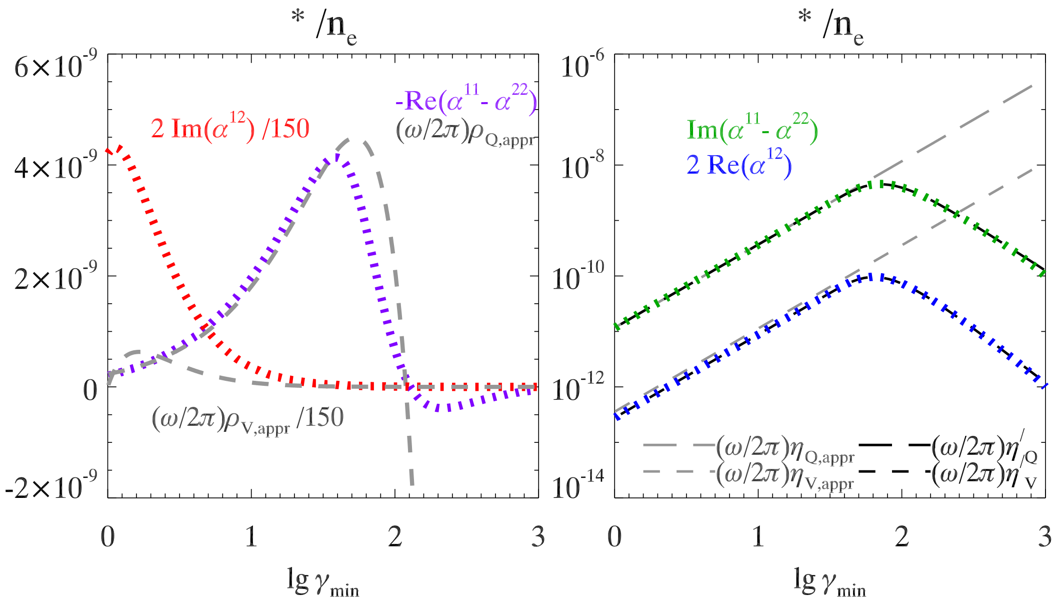

Figure 6. Propagation and absorption coefficients for power-law energy distribution with index $b = 2.5$. *Left*: Faraday rotation and conversion. Linear approximations by Melrose (1997b) are shown in grey dashed lines. *Right*: Absorption coefficients. Traditional synchrotron approximations are shown in black solid lines, whereas the approximations by Sazonov (1969) are shown in grey dashed lines.

4.2 New approximate formulae for Faraday conversion/rotation coefficients

We have shown that the traditional synchrotron approximations to the absorption coefficients are accurate and practical. On the contrary, simple linear approximations of the propagation coefficients have large errors at high electron energies. Although Sazonov (1969) also provided the integral expressions for the propagation coefficients in their Eq. (2.3), Jones & O'Dell (1977) in their Eq. (C16) as well, the Faraday rotation ($f^{(r)}$ therein) and especially Faraday conversion ($h^{(r)}$ therein) are inaccurate for high energies of electrons.

We devise a new set of approximate formulae for the complex response tensor in a plasma with monoenergetic particle distribution. The goal is to provide simple relations for accurate evaluation of propagation coefficients. We provide the numerical code in Mathematica 8 for the full evaluation at `http://astroman.org/Faraday_conversion/`, but we encourage the readers to use the simplified formulae for practical applications. These simplified formulae for Faraday rotation and Faraday conversion are computed for plasma with δ-function energy distribution. They can be easily integrated over the arbitrary energy distribution. Similar approximate formulae for thermal particle distributions were computed in Shcherbakov (2008).

4.2.1 Computations for monoenergetic particle distribution

It is non-trivial that good approximations to Faraday rotation/conversion coefficients exist in a three-dimensional parameter space of Ω_0/ω, θ, and γ. However, we manage to find the formulae accurate to within 10% at most reasonable combinations of parameters.

We define an auxiliary quantity

$$X_{\rm A} = \sqrt{\frac{\sqrt{2}\sin\theta}{10^{-4}}\frac{\Omega_0}{\omega}} \tag{53}$$

and introduce four new expressions: $H_{\rm X}$, $H_{\rm B}$, $g_{\rm X}$, and $g_{\rm B}$ to approximate $-{\rm Re}(\alpha^{11}-\alpha^{22})$, $-{\rm Re}(\alpha^{11}_{\rm B}-\alpha^{22}_{\rm B})$, $2{\rm Im}(\alpha^{12})$, and $2{\rm Im}(\alpha^{12}_{\rm B})$, respectively. The formulae are

$$H_{\rm X}(\gamma_0) \quad = \quad \begin{cases} 9.29\cdot 10^{-9}\cdot\sqrt{1-\gamma_0^{-1}}\cdot(X_{\rm A}\gamma_0)^{3.036}, & X_{\rm A}\gamma_0 < 40, \\ \\ -0.000203(X_{\rm A}\gamma_0)^{0.4343} - 0.0013\cos\left[0.5646\ln(X_{\rm A}\gamma_0) - 4.03\right] \\ +0.002\exp\left[-\frac{(\ln X_{\rm A}\gamma_0 - 4.2137)^2}{0.5429}\right] + 0.00083\exp\left[-\frac{(\ln X_{\rm A}\gamma_0 - 4.2137]^2}{0.2121}\right], & X_{\rm A}\gamma_0 \geqslant 40, \end{cases}$$

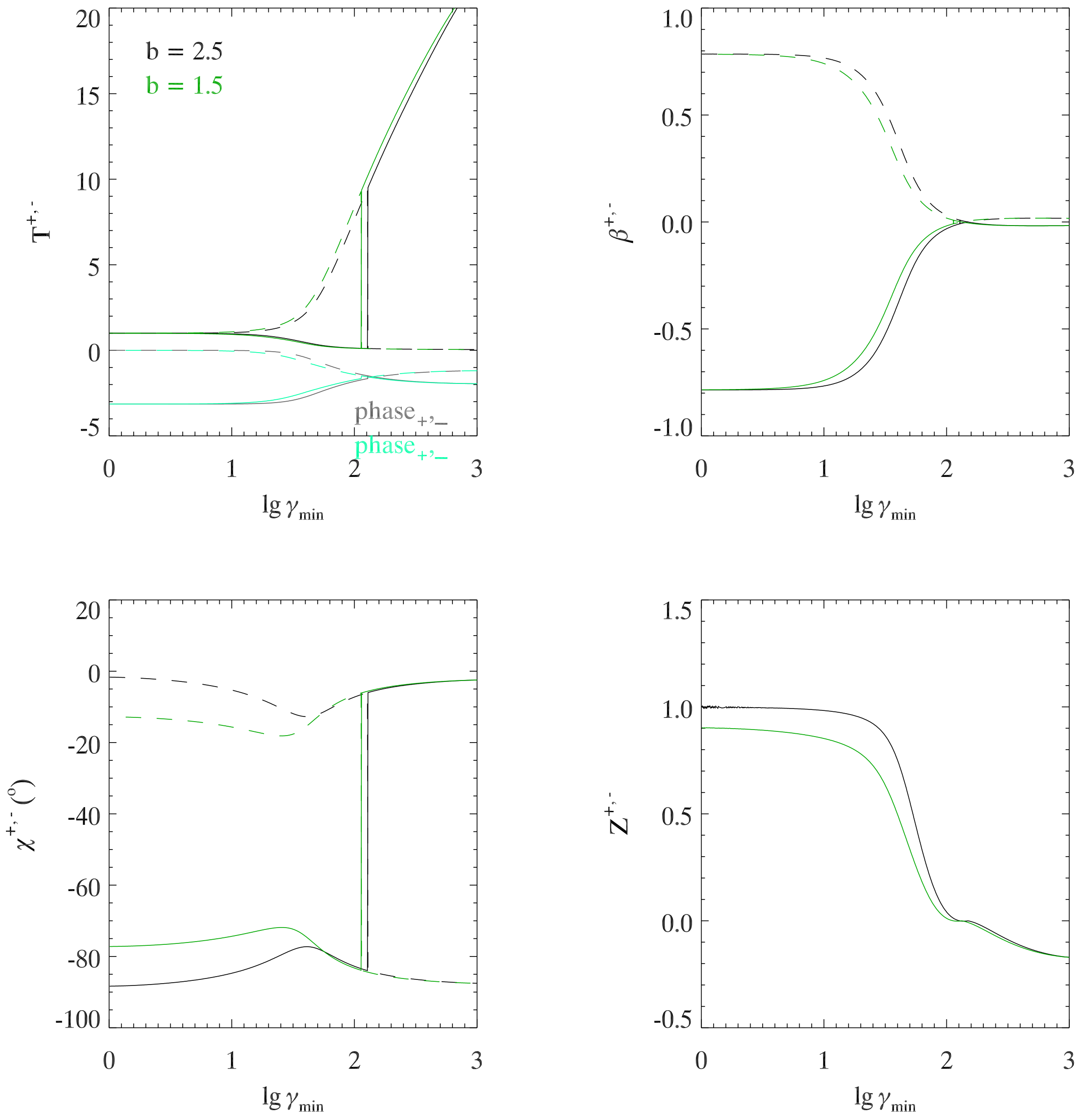

Figure 7. Properties of two natural modes for the power-law particle distribution. Amplitudes $T^{\pm}$ (black) and phases $\varphi^{\pm}$ (grey) of complex axial ratio, ellipticity $\beta^{\pm}$, EVPA $\chi^{\pm}$, and $Z^{+} = Z^{-}$ (eq. 33) are shown in four panels, respectively, for $b = 2.5$. Lines for $(^{+})$-mode are solid and for $(^{-})$-mode are dashed. The same quantities for the power-law distribution with $b = 1.5$ are shown in green and cyan.

$$
\begin{aligned}
H_{\mathrm{B}}(\gamma_0) &= \begin{cases} 4.67\cdot 10^{-9}\cdot(1-\gamma_0^{-1})^{\frac{3}{2}}\cdot(X_{\mathrm{A}}\gamma_0)^{3.84}, & X_{\mathrm{A}}\gamma_0 < 40, \\[2em] 0.864 - 0.2082\,(\ln X_{\mathrm{A}}\gamma_0)^2 + 0.0175\,(\ln X_{\mathrm{A}}\gamma_0)^4 - 0.000626\,(\ln X_{\mathrm{A}}\gamma_0)^6 & \\ \quad +1.0175\cdot 10^{-5}\,(\ln X_{\mathrm{A}}\gamma_0)^8 - 7.686\cdot 10^{-8}\,(\ln X_{\mathrm{A}}\gamma_0)^{10} & \\ \quad -0.01\exp\left[-\frac{(\ln X_{\mathrm{A}}\gamma_0-4.0755)^2}{0.0763}\right], & X_{\mathrm{A}}\gamma_0 \geqslant 40, \end{cases} \\
g_{\mathrm{X}}(\gamma_0) &= 1 - 0.4\exp\left[-\frac{(\ln X_{\mathrm{A}}\gamma_0 - 9.21)^2}{11.93}\right] - 0.05\exp\left[-\frac{(\ln X_{\mathrm{A}}\gamma_0 - 5.76)^2}{1.33}\right] + 0.075\exp\left[-\frac{(\ln X_{\mathrm{A}}\gamma_0 - 4.03)^2}{0.65}\right], \\
g_{\mathrm{B}}(\gamma_0) &= 1 - 0.0045(X_{\mathrm{A}}\gamma_0)^{0.52}. \qquad (54)
\end{aligned}
$$

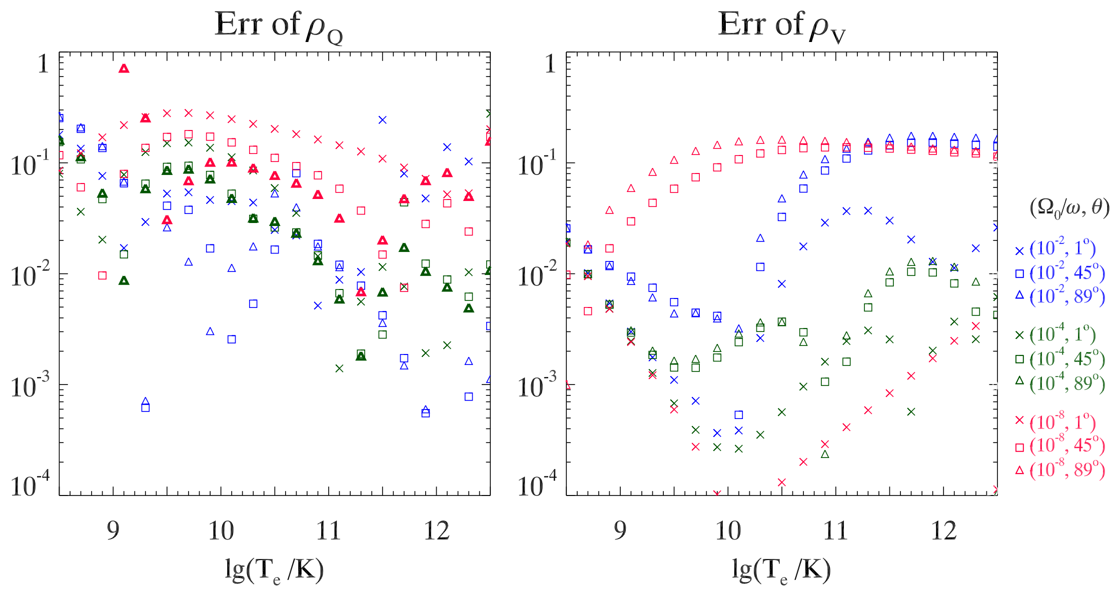

Figure 8. Accuracy checking for simplified formulae for Faraday conversion $\rho_{\rm Q}$ and Faraday rotation $\rho_{\rm V}$. See details in text.

The Faraday conversion/rotation coefficients for monoenergetic isotropic particle distribution with Lorentz factor γ_0 are calculated as

$$\begin{aligned}
\rho_Q(\gamma_0) &= -\frac{2\pi}{\omega}{\rm Re}(\alpha^{11}-\alpha^{22}) &&= \frac{8\pi^2 e^2}{m_e c\omega}\cdot X_{\rm A}\cdot H_{\rm X}(\gamma_0),\\
\rho_{Q,{\rm B}}(\gamma_0) &= -\frac{2\pi}{\omega}{\rm Re}(\alpha^{11}_{\rm B}-\alpha^{22}_{\rm B}) &&= \frac{8\pi^2 e^2}{m_e c\omega}\cdot H_{\rm B}(\gamma_0),\\
\rho_V(\gamma_0) &= 2\cdot\frac{2\pi}{\omega}{\rm Im}(\alpha^{12}) &&= \frac{8\pi^2 e^2\Omega_0\cos\theta}{m_e c\omega^2}\cdot\ln\left(\frac{1+p_0/\gamma_0}{1-p_0/\gamma_0}\right)\cdot g_{\rm X}(\gamma_0),\\
\rho_{V,{\rm B}}(\gamma_0) &= 2\cdot\frac{2\pi}{\omega}{\rm Im}(\alpha^{12}_{\rm B}) &&= \frac{8\pi^2 e^2\Omega_0\cos\theta}{m_e c\omega^2}\cdot\left[\gamma_0\cdot\ln\left(\frac{1+p_0/\gamma_0}{1-p_0/\gamma_0}\right)-2p_0\right]\cdot g_{\rm B}(\gamma_0).
\end{aligned}\tag{55}$$

Those for arbitrary particle distribution $f(\gamma)$ are calculated as

$$\begin{aligned}
\rho_Q &= \int_{\gamma_{\rm min}}^{\gamma_{\rm max}} f(\gamma)\cdot\rho_Q(\gamma){\rm d}\gamma - f(\gamma_{\rm max})\cdot\rho_{Q,{\rm B}}(\gamma_{\rm max}) + f(\gamma_{\rm min})\cdot\rho_{Q,{\rm B}}(\gamma_{\rm min}),\\
\rho_V &= \int_{\gamma_{\rm min}}^{\gamma_{\rm max}} f(\gamma)\cdot\rho_V(\gamma){\rm d}\gamma - f(\gamma_{\rm max})\cdot\rho_{V,{\rm B}}(\gamma_{\rm max}) + f(\gamma_{\rm min})\cdot\rho_{V,{\rm B}}(\gamma_{\rm min}).
\end{aligned}\tag{56}$$

The above formulae are accurate, with errors of several percent for δ-distribution in general. As a test, we choose $f(\gamma)$ in thermal distribution and calculate $(\omega/2\pi)\rho^T_{\rm Q}$ and $(\omega/2\pi)\rho^T_{\rm V}$ by them for a wide range of temperature. We then calculate $(\omega/2\pi)\rho^*_{\rm Q}$ and $(\omega/2\pi)\rho^*_{\rm V}$ by contour integrate formulae for thermal distribution, which is discussed in the Sec.4.2.2. The errors of $\rho_{\rm Q}$ are defined as $|(\omega/2\pi)\rho^T_{\rm Q}-(\omega/2\pi)\rho^*_{\rm Q}|/|(\omega/2\pi)\rho^*_{\rm Q}|$, and those of $\rho_{\rm V}$, similarly, as $|(\omega/2\pi)\rho^T_{\rm V}-(\omega/2\pi)\rho^*_{\rm V}|/|(\omega/2\pi)\rho^*_{\rm V}|$. I.e., error of 1 means the coefficient is accurate with a factor of 2. We choose nine couples of parameters $(\frac{\Omega_0}{\omega},\theta)$, such as $(10^{-2},1^\circ)$, $(10^{-2},45^\circ)$, $(10^{-2},89^\circ)$, $(10^{-4},1^\circ)$, $(10^{-4},45^\circ)$, $(10^{-4},89^\circ)$, $(10^{-8},1^\circ)$, $(10^{-8},45^\circ)$, and $(10^{-8},89^\circ)$, as examples represented by different symbols (cross, square, and triangle) and different color (blue, green, and red), respectively. As shown on Figure 8, the errors are less than 1 (100%) in general. For high temperatures at which synchrotron emission is effective ($>10^{10}$K), the errors are as good as within 0.1 (10%).

4.2.2 Results for thermal distribution

We have shown in § 4.1.1 that one can calculate the response tensor for monoenergetic particle first by integrating over the proper time (or phase), then integrate the result over the arbitrary particle distribution. For thermal distribution, one can change the integration order and analytically integrate over γ. Thus, the response tensor can be simplified to

$$\alpha^{ij}(k) = \frac{\imath n_e e^2}{m_e c \Theta_e^{-2} K_2(\Theta_e^{-1})} \int_0^\infty \mathrm{d}(\omega\xi) \left(\dot{t}^{ij}(\xi) \frac{K_2(\mathcal{R}'(\xi))}{\mathcal{R}'^2(\xi)} - \widetilde{T}^{ij}(\xi) \frac{K_3(\mathcal{R}'(\xi))}{\mathcal{R}'^3(\xi)} \right), \tag{57}$$

where

$$\mathcal{R}'(\xi) \;=\; \sqrt{\Theta_e^{-2} - 2\imath\Theta_e^{-1}\omega\xi + \frac{\omega^2\sin^2\theta}{\Omega_0^2}[2 - 2\cos(\Omega_0\xi) - \Omega_0^2\xi^2]}$$

and $\dot{t}^{ij}(\xi)$ and $\widetilde{T}^{ij}(\xi)$ are given in § 2.2. See the corresponding derivation in Appendix C, which closely follows Trubnikov (1958), Melrose (1997a), and Swanson (2003). The integrals for thermal $\alpha^{ij}(k)$ in Eq. (57) are easier to compute numerically. However, such simplification can only be done for thermal distribution. The detailed computations and discussion of Eq. 57 can be found in Shcherbakov (2008). Good fittings for thermal distribution, accurate within 10% except with large Ω_0/ω and large θ, are also provided therein. We will provide their expressions for electrons in a present notation[3]:

$$\begin{aligned}
X_e &= T_e\sqrt{\sqrt{2}\sin\theta\left(10^3\frac{\Omega_0}{\omega}\right)}, \\
\rho_{V,th} &= \frac{4\pi e^2\Omega_0}{m_e c\omega^2}\frac{K_0(T_e^{-1})}{K_2(T_e^{-1})}\cos\theta\cdot g(X_e), \\
\rho_{Q,th} &= \frac{2\pi e^2\Omega_0^2}{m_e c\omega^3}\left(\frac{K_1(T_e^{-1})}{K_2(T_e^{-1})} + 6T_e\right)\sin^2\theta\cdot h(X_e)
\end{aligned} \tag{58}$$

with approximate multipliers

$$\begin{aligned}
g(X_e) &= 1 - 0.11\ln(1 + 0.035X_e), \\
h(X_e) &= 2.011\exp\left(-\frac{X_e^{1.035}}{4.7}\right) - \cos\left(\frac{X_e}{2}\right)\exp\left(-\frac{X_e^{1.2}}{2.73}\right) - 0.011\exp\left(-\frac{X_e}{47.2}\right).
\end{aligned} \tag{59}$$

5 APPLICATIONS

We computed the response tensor in uniformly magnetized relativistic plasmas with isotropic particle distributions. We found Faraday conversion, Faraday rotation, and absorption coefficients by numerical integration in the complex plane. Then we discussed the properties of natural modes of cyclo-synchrotron radiation and presented the results for specific electron energy distributions. We provided accurate practical fitting formulae for Faraday conversion and rotation. The method of complex plane integration allows to calculate both absorption and propagation coefficients consistently. In practice, formulae in Sazonov (1969) are good enough for absorption coefficients. Therefore, we focus on improving the calculations of Faraday conversion and rotation coefficients. Faraday conversion and rotation coefficients can be generally expressed as $\rho_Q \propto h(\gamma, \lambda B, \theta) n_e B^2 \lambda^3$ and $\rho_V \propto g(\gamma, \lambda B, \theta) n_e B \lambda^2$, where h, g are functions of electron Lorentz factor γ, product of wavelength λ and magnetic field $B = |\boldsymbol{B}|$, and angle θ between wavevector $\boldsymbol{k}$ and magnetic field $\boldsymbol{B}$.

Previous work (e.g., Melrose 1997b; Quataert & Gruzinov 2010) has shown that $g \approx 1$, if $\gamma \approx 1$ for typical λ, B, θ, but $g \ll 1$ if $\gamma \gg 1$. This means the Faraday rotation becomes less important, when the electrons become relativistic. Therefore, the direction of LP plane changes little. Our calculations suggest the function g and the Faraday rotation coefficient were previously computed precisely, but function h and Faraday conversion coefficient were not. The function h grows from small to intermediate γ, but h steeply decreases, if γ grows more. This means the Faraday conversion also becomes less important when the electrons become relativistic, although the peak Lorentz factor depends on frequency ratio Ω_0/ω and the particle distribution. In sum, as the absorption coefficients at a given frequency ω also decrease with γ, ultrarelativistic electrons interact less with radiation field.

We have shown that Faraday conversion coefficient should be computed more precisely. Let us now demonstrate that imprecise estimates of propagation effects result in large error in polarized simulated fluxes for accretion onto compact objects. We compare polarized spectra for two cases: accurate general relativistic polarized radiative transfer (Shcherbakov & Huang 2011) and assuming that Faraday conversion and rotation coefficients are given by linear approximations. We test two types of dynamical models for Sgr A* accretion to prove the case. Both models assume thermal electron distribution.

First, we adopt the analytic model from Huang, Takahashi & Shen (2009). This model is established for Sgr A* based on radiatively inefficient accretion flow (RIAF) solution with different temperatures in ions and electrons. It reasonably fits Sgr A* polarized mm/sub-mm spectrum. On the left panel of Figure 9 we plot the accurate ratio ρ_Q/ρ_V (solid lines) and the ratio $\rho_{Q,\mathrm{lin}}/\rho_{V,\mathrm{lin}}$ in linear approximation (dashed lines) as functions of electron temperature T_e for $\Omega_0/\omega = 10^{-4}$ and

---

[3] Note, that the basis vectors in Shcherbakov (2008) are different, thus a different sign of ρ_Q.

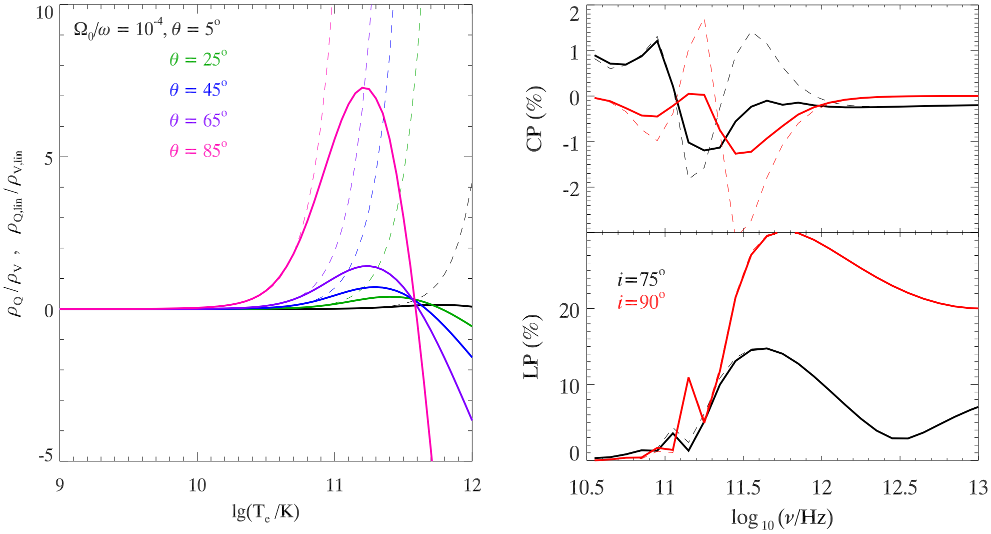

Figure 9. *Left*: Examples of accurate ratios of ρ_Q/ρ_V (solid) and their linear approximations $\rho_{Q,\rm lin}/\rho_{V,\rm lin}$ (dashed) for thermal electrons with $\Omega_0/\omega = 10^{-4}$ and different θ. *Right*: Simulated CP and LP fluxes based on accurate Faraday conversion/rotation (solid) and their linear approximations (dashed) for Sgr A* accretion model in (Huang, Takahashi & Shen 2009) with inclination angle of 75° (black) and 90° (red).

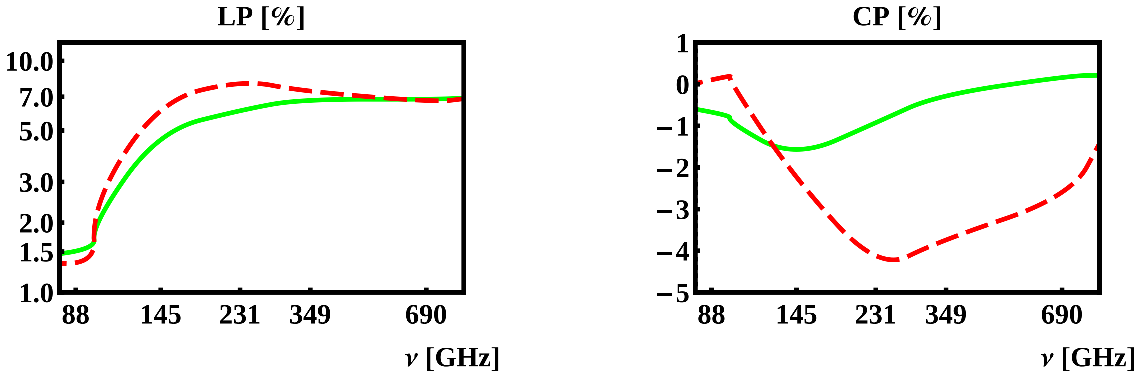

Figure 10. Simulated LP (on the *left*) and CP (on the *right*) fractions for Sgr A* for various prescriptions of Faraday rotation and Faraday conversion: for linear approximations $\rho_{Q,\rm lin}/\rho_{V,\rm lin}$ (dashed red) and for accurate ρ_V and ρ_Q (solid green). We employ the best-fitting dynamical model from Shcherbakov et al. (2010) with dimensionless spin $a_* = 0.9$.

different $\boldsymbol{k}-\boldsymbol{B}$ angles. On the right panel, we plot simulated circular and linear polarization spectra computed with accurate Faraday conversion and rotation coefficients (solid lines) and the results for the same dynamical model for assumed linear approximations of propagation coefficients (dashed lines). The inclination angles of the disk $i = 75°$ (black) and $i = 90°$ (red) are chosen.

The frequency ratio $\Omega_0/\omega \sim 10^{-4}$ corresponds to sub-millimeter band close to the event horizon of Sgr A*. There the electron temperature is $T_e \sim 10^{10.5-11.5}$K. The Faraday conversion becomes strong ($\rho_Q/\rho_V > 1$) at large angles $\theta > 45°$. One can also note from the right panel of Figure 4 that η_V absorption coefficient is less than 1% of η_I. Therefore emissivity in V is equally weak according to Kirchhoff's Law. So Faraday conversion plays a major role in the production of circular polarization. However, ρ_Q/ρ_V reaches a peak at a specific temperature around 10^{11}K then decreases again, while $\rho_{Q,\rm lin}/\rho_{V,\rm lin}$ monotonically increases to much greater than 1. Therefore, the amplitudes of circular polarization predicted for accurate (ρ_Q, ρ_V) are less than half of those predicted for approximate $(\rho_{Q,\rm lin}, \rho_{V,\rm lin})$, although accurate and simplified propagation coefficients predict similar linear polarization.

Changes in simulated polarized fluxes are shown on Figure 10 for the best-fitting Sgr A* accretion model from Shcherbakov et al. (2010). This model is inspired by three-dimensional general relativistic magneto hydrodynamic simulations. The structure of magnetic field, velocity and density fields are taken directly from simulations. All free parameters are adjusted to achieve the best fit. Similarly to aforementioned analytic model, circular polarization in sub-millimeter band is significantly lower, when the precise Faraday conversion and rotation coefficients are adopted for the same dynamical model. Thus substantially lower predicted CP fractions, when the precise propagation coefficients are adopted, is a generic model-independent result. Our calculation showed that linear approximations of Faraday conversion/rotation are invalid for electrons with such high energy. They significantly overestimate the circular polarization for the relevant range of ratios Ω_0/ω. When fitting polarized observations and predicting polarized spectra one should adopt accurate Faraday conversion and rotation coefficients computed in § 2.2 or the simplified fitting formulae provided in § 4.2.

The validity of linear approximations of Faraday conversion and rotation coefficients depends not only on the energy of electrons, but also on the frequency ratio Ω_0/ω. The observational frequency in near IR (NIR) is $\sim 10^3$ larger than that in sub-mm. The typical frequency ratio Ω_0/ω is around $10^{-6} - 10^{-8}$, which yields the values of (ρ_Q, ρ_V) similar to those of $(\rho_{Q,\rm lin}, \rho_{V,\rm lin})$ for $\gamma < 50$. Thus, the linear approximations of Faraday conversion and rotation coefficients still adequately describe the correspondent effects in NIR.

Observations of sub-mm circular polarization from Sgr A* are one of today's big interests and challenges. CP fraction is only about 1% in sub-mm, but was already detected at several frequencies (Munoz et al. 2011). Still, there is substantial spread between different Sgr A* models (Shcherbakov et al. 2010) in CP fluxes at frequencies, where CP flux was not yet measured, for example 88 GHz, 145 GHz, and 690 GHz. Observations at these frequencies can help to further discriminate between models of various types, which have different black hole spins.

ACKNOWLEDGMENTS

The authors are grateful to Prof. Makoto Inoue, Dr. Rohta Takahashi, and Prof. Ramesh Narayan for useful suggestions. **The comments of anonymous referee helped to improve presentation of findings.** This work was supported in part by the National Natural Science Foundation of China (grants 10625314, 10633010 and 10821302), the Knowledge Innovation Program of the Chinese Academy of Sciences (Grant No. KJCX2-YW-T03), the National Key Basic Research Development Program of China (No. 2007CB815405), and the CAS/SAFEA International Partnership Program for Creative Research Teams. LH acknowledges the support by China Postdoctoral Science Foundation (grant 20090450822) and Regular Postdoctoral Research Fellowship in Academia Sinica. RVS acknowledges the support by NASA grants NNX08AX04H and NNX11AE16G.

REFERENCES

Ballantyne D. R., Ozel F., Psaltis D., 2007, ApJ, 663, L17
Beckert T., 2003, Ap& SS, 288, 123
Bower G. C., Falcke H., Sault R. J., & Backer D. C., 2002, ApJ, 571, 843
Bower G. C., Falcke H., Wright M. C. H., & Backer D. C., 2005, ApJ, 618, L29
Ginzburg V. L., 1964, Soviet Physics Doklady, 9, 329
Homan D. C., Lister M. L., Aller, H. D., Aller, M. F., & Wardle, J. F. C., 2009, ApJ, 696, 328
Huang L., Liu S., Shen Z.-Q., Yuan Y.-F., Cai M. J., Li H., Fryer C. L., 2009, ApJ, 703, 557
Huang L., Takahashi R., Shen Z. -Q., 2009, ApJ, 706, 960
Landi DeglInnocenti, E., & Landolfi, M. 2004, Polarization in Spectral Lines (Dordrecht: Kluwer)
Jones T. W., O'Dell S. L., 1977, ApJ, 214, 522
Landau L. D., Lifshits E. M., 1980, "Physical Kinetics" (Oxford: Pergamon Press)
Legg M. P. C., Westfold K. C., 1968, ApJ, 154, 499
Melrose D. B., 1997a, J. Plasma Physics, 57, 479
Melrose D. B., 1997b, J. Plasma Physics, 58, 735
Melrose D. B., 2010, J. Quantum Plasmadynamics: Magnetized Plasmas (Springer)
Munoz, D. J., Marrone, D. P., Moran, J. M., Rao R. 2011, ApJ, submitted
Pacholczyk A. G., 1970, "Radio astrophysics. Nonthermal processes in galactic and extragalactic sources", (Freeman: San Francisco)
Quataert E., Gruzinov A., 2000, ApJ, 545, 842
Sazonov V. N., 1969, Soviet Astronomy, 13, 396
Shcherbakov R. V., 2008, ApJ, 688, 695
Shcherbakov R., Huang L., 2011, MNRAS, 410, 1052
Shcherbakov, R. V., Penna, R. F., McKinney, J. C. 2010, ApJ submitted, astro-ph/1007.4832
Swanson D. G., 2003, "Plasma waves" (Bristol: Institute of Physics Pub.)

Trubnikov B. A., 1958, "Magnetic emission of high temperature plasma". Thesis, Moscow Institute of Engineering and Physics [English translation in AEC-tr-4073, US Atomic Energy Commission, Oak Ridge, Tennessee, 1960]. B.A. Trubnikov.
Yuan F., Quataert E., Narayan R., 2003, ApJ, 598, 301

Appendix A: Definitions and derivations

Here we summarize all definitions and derivations related to the response tensor. They are similar to those in (Melrose 1997a,b), except for the signature of the metric tensor and the geometry of the coordinate system. We list all related tensors which are different from those in Melrose's work.

Metric tensor in Minkowski space-time: $g^{\mu\nu} = \mathrm{diag}[-1, 1, 1, 1]$.
Wave vector: $k^\mu = \omega(1, 0, 0, 1)^{\mathrm{T}}$.
Tensor of magnetostatic field:

$$F_0^{\mu\nu} = Bf^{\mu\nu}, \qquad B \quad = \quad \left(\frac{1}{2}F_0^{\mu\nu}F_{0\mu\nu}\right)^{1/2}, \qquad f_{\mu\nu} = \begin{pmatrix} 0 & 0 & 0 & 0 \\ 0 & 0 & \cos\theta & \sin\theta \\ 0 & -\cos\theta & 0 & 0 \\ 0 & -\sin\theta & 0 & 0 \end{pmatrix}.$$

Auxiliary tensor for electron velocity perturbations:

$$\dot{t}^{\mu\nu}(\tau) = \begin{pmatrix} -1 & 0 & 0 & 0 \\ 0 & \cos\Omega_0\tau & -\cos\theta\sin\Omega_0\tau & -\sin\theta\sin\Omega_0\tau \\ 0 & \cos\theta\sin\Omega_0\tau & \sin^2\theta + \cos^2\theta\cos\Omega_0\tau & -\sin\theta\cos\theta + \sin\theta\cos\theta\cos\Omega_0\tau \\ 0 & \sin\theta\sin\Omega_0\tau & -\sin\theta\cos\theta + \sin\theta\cos\theta\cos\Omega_0\tau & \cos^2\theta + \sin^2\theta\cos\Omega_0\tau \end{pmatrix}.$$

Auxiliary tensor for electron position perturbations:

$$T^{\mu\nu}(\tau) = t^{\mu\nu}(\tau) - t^{\mu\nu}(0) = \begin{pmatrix} -\tau & 0 & 0 & 0 \\ 0 & \frac{\sin\Omega_0\tau}{\Omega_0} & -\cos\theta\frac{1-\cos\Omega_0\tau}{\Omega_0} & -\sin\theta\frac{1-\cos\Omega_0\tau}{\Omega_0} \\ 0 & \cos\theta\frac{1-\cos\Omega_0\tau}{\Omega_0} & \sin^2\theta\tau + \cos^2\theta\frac{\sin\Omega_0\tau}{\Omega_0} & -\sin\theta\cos\theta\tau + \sin\theta\cos\theta\frac{\sin\Omega_0\tau}{\Omega_0} \\ 0 & \sin\theta\frac{1-\cos\Omega_0\tau}{\Omega_0} & -\sin\theta\cos\theta\tau + \sin\theta\cos\theta\frac{\sin\Omega_0\tau}{\Omega_0} & \cos^2\theta\tau + \sin^2\theta\frac{\sin\Omega_0\tau}{\Omega_0} \end{pmatrix}.$$

In 6-dimensional phase space: electron velocity v, electron momentum m_ep, and distribution function of electrons f(p).
In 8-dimensional phase space: Lorentz factor $\gamma = 1/\sqrt{1-|\mathrm{v}|^2}$, velocity of electron $\mathcal{U}^\mu = (\gamma, \mathrm{u}) = (\gamma, \gamma\mathrm{v})$, momentum $\mathcal{P}^\mu = (\gamma m_e, m_e\mathrm{p}) = (\gamma m_e, \gamma m_e\mathrm{v})$, and distribution function of electrons $\mathcal{F}(\mathcal{P}) = 2m_e\delta\left(\mathcal{P}^2 + m_e^2\right)\mathrm{f}(\mathrm{p})$.
The general form of the response tensor for an arbitrary isotropic distribution of electrons is

$$\alpha^{\mu\nu}(k) = \imath e^2 \int \mathrm{d}^4\mathcal{P}(\tau) \int_0^\infty \mathrm{d}\xi \cdot \mathcal{U}^\mu(\tau) e^{\imath k[X(\tau-\xi)-X(\tau)]} k\mathcal{U}(\tau-\xi) \left(g^{\lambda\nu} - \frac{k^\lambda\mathcal{U}^\nu(\tau-\xi)}{k\mathcal{U}(\tau-\xi)}\right) \dot{t}_\lambda^\sigma(\tau-\xi) \frac{\partial\mathcal{F}(\mathcal{P})}{\partial\mathcal{P}^\sigma(0)}.$$

Appendix B: Derivation of the response tensor for monoenergetic particle distribution

Let us introduce $\widetilde{\mathcal{U}}^\mu = [1, 0, 0, 0]$ — 4-velocity in the rest frame of plasma. Then

$$\begin{aligned}
\alpha^{\mu\nu}(k) \quad &= \quad \imath e^2 \int \mathrm{d}^4\mathcal{P}(\tau) \\
&\times \quad \int_0^\infty \mathrm{d}\xi \mathcal{U}^\mu(\tau) e^{\imath k[X(\tau-\xi)-X(\tau)]} k\mathcal{U}(\tau-\xi) \left(g^{\lambda\nu} - \frac{k^\lambda\mathcal{U}^\nu(\tau-\xi)}{k\mathcal{U}(\tau-\xi)}\right) \dot{t}_\lambda^\sigma(\tau-\xi) \left[2m_e\delta\left(\mathcal{P}^2 + m_e^2\right)\right] m_e^{-3} \frac{\partial\mathrm{f}(\gamma)}{\partial\mathcal{P}^\sigma(0)} \\
&= \quad \imath e^2 \int \mathrm{d}^4\mathcal{P}(\tau) \\
&\times \quad \int_0^\infty \mathrm{d}\xi \mathcal{U}^\mu(\tau) e^{\imath k[X(\tau-\xi)-X(\tau)]} k\mathcal{U}(\tau-\xi) \left(g^{\lambda\nu} - \frac{k^\lambda\mathcal{U}^\nu(\tau-\xi)}{k\mathcal{U}(\tau-\xi)}\right) \dot{t}_\lambda^\sigma(\tau-\xi) \widetilde{\mathcal{U}}_\sigma \left[2m_e\delta\left(\mathcal{P}^2 + m_e^2\right)\right] m_e^{-4} \frac{\mathrm{df}(\gamma)}{\mathrm{d}\gamma} \\
&= \quad \frac{\imath e^2}{m_e} \int \mathrm{d}^4\mathcal{P}(\tau) \left[2m_e\delta\left(\mathcal{P}^2 + m_e^2\right)\right] m_e^{-3} \frac{\mathrm{df}(\gamma)}{\mathrm{d}\gamma} \int_0^\infty \mathrm{d}\xi \mathcal{U}^\mu(\tau) e^{\imath k[X(\tau-\xi)-X(\tau)]} \left[k\mathcal{U}(\tau-\xi)\widetilde{\mathcal{U}}^\nu - k\widetilde{\mathcal{U}}\mathcal{U}^\nu(\tau-\xi)\right] \\
&\qquad (\text{let} \quad \tau = 0) \\
&= \quad -\frac{e^2}{m_e} \int \mathrm{d}^4\mathcal{P}(\tau) \left[2m_e\delta\left(\mathcal{P}^2 + m_e^2\right)\right] m_e^{-3} \frac{\mathrm{df}(\gamma)}{\mathrm{d}\gamma} \left[\mathcal{U}^\mu\widetilde{\mathcal{U}}^\nu + \imath k\widetilde{\mathcal{U}} \int_0^\infty \mathrm{d}\xi \mathcal{U}^\mu \dot{t}^{\nu\sigma}(-\xi)\mathcal{U}_\sigma e^{\imath k_\lambda T^{\lambda\sigma}(-\xi)\mathcal{U}_\sigma}\right] \\
&= \quad -\frac{e^2}{m_e} \int \mathrm{d}^3\mathrm{p} \left(\frac{1}{\gamma}\right) \frac{\mathrm{df}(\gamma)}{\mathrm{d}\gamma} \left[\mathcal{U}^\mu\widetilde{\mathcal{U}}^\nu + \imath k\widetilde{\mathcal{U}} \int_0^\infty \mathrm{d}\xi \mathcal{U}^\mu \dot{t}^{\nu\sigma}(-\xi)\mathcal{U}_\sigma e^{-\imath k_\lambda T^{\sigma\lambda}(\xi)\mathcal{U}_\sigma}\right]
\end{aligned}$$

$$= \quad -\frac{e^2}{m_e c} \int \mathrm{d}^3\mathrm{p} \frac{\mathrm{d}f(\gamma)}{\mathrm{d}\gamma} \widetilde{\mathcal{U}}^\mu\widetilde{\mathcal{U}}^\nu + \frac{\imath e^2\omega}{m_e c} \int_0^\infty \mathrm{d}\xi \dot{t}_\sigma^\nu(-\xi) \frac{\partial^2}{\partial\mathcal{S}_\mu\partial\mathcal{S}_\sigma} \left[\int \mathrm{d}^3\mathrm{p} \left(-\frac{1}{\gamma}\frac{\mathrm{d}f(\gamma)}{\mathrm{d}\gamma} \mathrm{e}^{-\imath\mathcal{R}(\xi)\mathcal{U} + \mathcal{S}\mathcal{U}}\right)\right]_{\mathcal{S}_\mu = 0}, \tag{1}$$

which coincides with Eq. 9. We denoted $\mathcal{R}^{\mu}(\xi) = k_{\lambda} T^{\mu\lambda}(\xi)$ and introduced an auxiliary variable $\mathcal{S}_{\mu}$.

Appendix C: Derivation of the response tensor for thermal particle distribution

Substituting the thermal distribution into Eq. 12 we obtain

$$I(\xi, s) = \frac{n_e}{\Theta_e K_2(\Theta_e^{-1})} \int_1^{+\infty} \mathrm{e}^{-(\Theta_e^{-1} - \imath\omega\xi + s_0)\gamma} \left[(\imath\omega\xi + s_0) \cdot \frac{\sin\left(|\mathbf{R} + \imath\mathbf{s}||\mathbf{p}|\right)}{|\mathbf{R} + \imath\mathbf{s}|} + \frac{\gamma}{\sqrt{\gamma^2 - 1}} \cdot \cos\left(|\mathbf{R} + \imath\mathbf{s}||\mathbf{p}|\right) \right] \mathrm{d}\gamma, \tag{1}$$

where $|\mathbf{p}| = \sqrt{\gamma^2 - 1}$. We can simplify the above formula as follows:

$$\begin{aligned}
\frac{\Theta_e K_2(\Theta_e^{-1})}{n_e} \cdot I(\xi, s) \quad &= \quad \left[-\frac{\imath\omega\xi + s_0}{(\Theta_e^{-1} - \imath\omega\xi + s_0)} - 1 \right] \int_0^{+\infty} \frac{\sin(|\mathbf{R} + \imath\mathbf{s}||\mathbf{p}|)}{|\mathbf{R} + \imath\mathbf{s}|} \cdot \mathrm{d}\mathrm{e}^{-(\Theta_e^{-1} - \imath\omega\xi + s_0)\gamma} \\
&= \quad \frac{1}{(\Theta_e^{-1} - \imath\omega\xi + s_0)} \int_0^{+\infty} \mathrm{e}^{-(\Theta_e^{-1} - \imath\omega\xi + s_0)\gamma} \cos(|\mathbf{R} + \imath\mathbf{s}||\mathbf{p}|) \cdot \mathrm{d}|\mathbf{p}| \\
&= \quad \frac{1}{2(\Theta_e^{-1} - \imath\omega\xi + s_0)} \int_{-\infty}^{+\infty} \mathrm{e}^{-(\Theta_e^{-1} - \imath\omega\xi + s_0)\gamma} \cdot \mathrm{e}^{|\mathbf{R} + \imath\mathbf{s}||\mathbf{p}|} \cdot \mathrm{d}|\mathrm{p}| \\
& \quad\quad (\text{let} \quad |\mathbf{p}| = \sinh z, \quad \gamma = \cosh z) \\
&= \quad \frac{1}{2(\Theta_e^{-1} - \imath\omega\xi + s_0)} \int_{-\infty}^{+\infty} \mathrm{e}^{-(\Theta_e^{-1} - \imath\omega\xi + s_0)\cosh z + |\mathbf{R} + \imath\mathbf{s}| \sinh z} \cosh z \mathrm{d}z \\
&= \quad \frac{\partial}{\partial(\Theta_e^{-1} - \imath\omega\xi + s_0)^2} \int_{-\infty}^{+\infty} \mathrm{d}z \quad \mathrm{e}^{-\sqrt{(\Theta_e^{-1} - \imath\omega\xi + s_0)^2 + |\mathbf{R} + \imath\mathbf{s}|^2} \cosh\left[z - \imath \tan^{-1}\left(\frac{|\mathbf{R} + \imath\mathbf{s}|}{\Theta_e^{-1} - \imath\omega\xi + s_0} \right) \right]} \\
&= \quad \frac{\partial}{\partial(\Theta_e^{-1} - \imath\omega\xi + s_0)^2} \left[2K_0 \left(\sqrt{(\Theta_e^{-1} - \imath\omega\xi + s_0)^2 + |\mathbf{R} + \imath\mathbf{s}|^2} \right) \right] \\
& \quad\quad \left(\quad \text{let} \quad \mathcal{R}'(\xi) = \sqrt{(\Theta_e^{-1} - \imath\omega\xi + s_0)^2 + |\mathbf{R} + \imath\mathbf{s}|^2} \quad \right) \\
&= \quad \frac{K_1\left(\mathcal{R}'(\xi)\right)}{\mathcal{R}'(\xi)}.
\end{aligned} \tag{2}$$

Following Eq. 9 and using

$$\frac{1}{\mathcal{R}'(\xi)} \frac{\mathrm{d}}{\mathrm{d}\mathcal{R}'(\xi)} \left[\frac{K_n(\mathcal{R}'(\xi))}{\mathcal{R}'(\xi)^n} \right] \quad = \quad -\frac{K_{n+1}(\mathcal{R}'(\xi))}{\mathcal{R}'(\xi)^{n+1}}$$

we have

$$\alpha^{ij}(k) = \frac{\imath n_e e^2}{m_e c \Theta_e^{-2} K_2(\Theta_e^{-1})} \int_0^{\infty} \mathrm{d}(\omega\xi) \left(\dot{t}^{ij}(\xi) \frac{K_2(\mathcal{R}'(\xi))}{\mathcal{R}'^2(\xi)} - \widetilde{T}^{ij}(\xi) \frac{K_3(\mathcal{R}'(\xi))}{\mathcal{R}'^3(\xi)} \right), \tag{3}$$

which is Eq. 57.